Characterization of potential biophysical regulators for clustering of the multifunctional lipid $PI(4,5)P_2$

Raquel Alexandra Bispo Guerreiro

Thesis to obtain the Master of Science Degree in

Biotechnology

Supervisor: Dr. Fábio Monteiro Fernandes

Co-Supervisor: Dr. Sandra Cristina Nunes Trigo Fernandes Pinto

Examination Committee

Chairperson: Dr. Nuno Gonçalo Pereira Mira

Supervisor: Dr. Fábio Monteiro Fernandes

Member of the Committee: Dr. Maria João Martins Sarmento

October 2021

Declaration

I declare that this document is an original work of my own authorship and that it fulfills all the requirements of the Code of Conduct and Good Practices of the Universidade de Lisboa.

Preface

The work presented in this thesis was performed at the Institute for of Instituto superior Técnico (Lisbon, Portugal), during the period September-October 2020/2021, under the supervision of Dr. Fábio Fernandes and co-supervised by Dr. Sandra Pinto.

Acknowledgements

I would like to start by thanking my supervisors, Dr. Fábio Fernandes and Dr. Sandra Pinto for the opportunity they gave me and for their support. Specially, I would like to thank Fabio for guiding me this year, for being always present and especially for the patience he showed me.

I would like to express my gratitude to iBB for the support and help whenever I needed.

To my partner Rita, you were the person who has been there since the day we started this journey, thank you for your affection, for your friendship, for your support. You were the best I could have asked for.

To my friends “Capítulo V” the biggest thanks, for being the people who were there every day for me, for making me believe that it was possible to get here, for showing me that Alentejo, Landim and Lisbon together could make five strong people united and prepared for the future. I'm very proud of us.

To my friends Nádia and Caixeiro, for being by my side for so many years, for your friendship, for your support, for your hugs.

To my partner in life, thank you for never letting me give up, for always believing in me, for being my pillar, for always making me see the positive side, for being by my side in all victories and defeats. Thank you for being yourself.

To my parents, for being there for me every time, for allowing the dream to become a reality. For their unconditional love and support. A huge thank to my father, for fighting with me all these years, for always taking the time to listen to me, for all the support, for all the times you were on call talk to me so I wouldn't feel lonely. I am very proud to be your daughter.

Lastly, I want to thank my sister and brother, for showing me how happiness can be in the little things, for making me fight and wanting to be a better person every day. I hope I made you proud.

Resumo

$PI(4,5)P_2$ é um importante fosfoinositol, localizado no folheto interno da membrana plasmática das células eucariotas. Neste fosfolípido, o seu grupo inositol encontra-se fosforilado nas posições 4 e 5, conferindo ao fosfolípido uma elevada carga negativa. $PI(4,5)P_2$ tem um papel fundamental na regulação da dinâmica da membrana plasmática, onde interage com um elevado número de proteínas e tem um papel crítico na sua regulação, participando ainda como substrato na produção de segundos mensageiros em várias vias de sinalização.

A interação de catiões divalentes com $PI(4,5)P_2$, tem a capacidade de alterar dramaticamente a organização deste fosfolípido. O cálcio é um ião divalente, com uma concentração intracelular extremamente baixa e altamente regulada. Tendo em conta o efeito dramático de pequenas variações dos níveis de Ca^{2+} na organização do $PI(4,5)P_2$, é provável que este fenómeno desempenhe uma papel importante nas vias de sinalização associadas a variações da concentração de Ca^{2+}. Por outro lado, a agregação de $PI(4,5)P_2$ é observada também a níveis fisiológicos de Mg^{2+}, o que sugere que a agregação pode apresentar um caráter constitutivo, tendo impactos consideráveis na atividade do $PI(4,5)P_2$.

Muito recentemente, estudos revelaram um surpreendente papel da reorganização do $PI(4,5)P_2$ na modulação do metabolismo lipídico, particularmente em resposta a stress térmico ou associado a choques osmóticos, sugerindo que a distribuição de $PI(4,5)P_2$ é influenciada pela temperatura e pela tensão de membrana. Nesta tese procurou-se avaliar a relevância de diferentes variáveis no processo de agregação do $PI(4,5)P_2$. Os parâmetros avaliados foram a temperatura, a concentração de colesterol e a tensão de membrana.

Os resultados demonstraram que a agregação de $PI(4,5)P_2$ é largamente independente da energia térmica ou da tensão de membrana. Para além disso, na gama de concentrações de colesterol estudada aqui, o colesterol revelou-se incapaz de inibir a formação de domínios gel de $PI(4,5)P_2$ induzidos pelo cálcio. A estabilidade dos complexos de $PI(4,5)P_2$ aparenta portanto ser maior do que inicialmente esperado. Nestas condições, o equilíbrio entre $PI(4,5)P_2$ monovalente e agregado, será largamente ditado pela concentração de proteínas com grande afinidade pelo lípido e com capacidade de sequestrarem $PI(4,5)P_2$. Por outro lado, a concentração de $PI(4,5)P_2$ livre deverá ser residual.

Palavras-chave

$PI(4,5)P_2$

Cálcio

Tensão de membrana

Colesterol

Abstract

$PI(4,5)P_2$ is an important phosphoinositol, located in the internal leaflet of the eukaryotic cell plasma membrane. In this phospholipid, the inositol group is phosphorylated in positions 4 and 5, giving the phospholipid a high negative charge. $PI(4,5)P_2$ has a fundamental role in regulating the dynamics of the plasma membrane, in events such as exocytosis/endocytosis and participates as a substrate in the production of second messengers in various signalling pathways.

The interaction of divalent cations with $PI(4,5)P_2$, has the capacity to dramatically change the organization of this phospholipid. Calcium is a divalent ion, with an extremely low and highly regulated intracellular concentration. $PI(4,5)P_2$ has high affinity for Ca^{2+} and in its presence forms aggregates on lipid membranes. Taking into account the dramatic effect of small variations in Ca^{2+} levels in the organization of $PI(4,5)P_2$, this phenomenon is likely to play an important role in signalling pathways associated with variations in Ca^{2+} concentration. On the other hand, the aggregation of $PI(4,5)P_2$ is also observed at physiological levels of Mg^{2+}, which suggests that the aggregation may have a constitutive character, having considerable impacts on the activity of $PI(4,5)P_2$.

Recently, various studies have revealed a surprising role for the reorganization of $PI(4,5)P_2$ in the modulation of lipid metabolism, particularly in response to thermal stress or associated with osmotic shock, suggesting that the distribution of PI(4,5)P2 is influenced by temperature and by membrane tension. In this thesis, we wanted to assess the relevance of different variables in the process of aggregation of $PI(4,5)P_2$. The parameters evaluated were temperature, cholesterol concentration and membrane tension.

The results demonstrated that the aggregation of $PI(4,5)P_2$ is largely independent of thermal adaptation or membrane tension. Furthermore, in the range of cholesterol concentrations studied in this work, cholesterol was unable to inhibit calcium-induced formation of $PI(4,5)P_2$ gel domains. The stability of $PI(4,5)P_2$ complexes therefore appears to be greater than initially expected. Under these conditions, the balance between both monovalent and aggregated $PI(4,5)P_2$ will be largely dictated by the concentration of proteins with high affinity for the lipid and capable of sequestering $PI(4,5)P_2$. On the other hand, the concentration of free $PI(4,5)P_2$ should be residual.

Keywords:

$PI(4,5)P_2$

Calcium

Membrane tension

Cholesterol

Table of Contents

List of Figures

List of Tables

List of Symbol

a	Radius of the particle
D	Diffusion coefficient
E	FRET efficiency
f(κa)	Henry function
G	Calibration factor
I	Fluorescence intensity
I_{VV}	Fluorescence intensities of the vertical components
I_{VH}	Fluorescence intensities of the horizontal components
I_{HV}	Fluorescence intensities of vertically polarized light
I_{HH}	Fluorescence intensities of vertically polarized light
$Int(CF)_{in}$	Average fluorescence intensity inside each vesicle
$Int(CF)_{out}$	Average fluorescence intensity outside each vesicle
$\boldsymbol{i(t)}$	Fluorescence intensity decay
κ	Debye length
kd	Dissociation rate constant
<*r*>	Steady-state fluorescence anisotropy
R_0	Förster radius
z	Zeta potential
$\boldsymbol{U_e}$	Electrophoretic mobility
η	Solution viscosity
λ	Wavelength
α_i	Normalized amplitude i
Δ<r>	Difference between fluorescence anisotropy values
ε	Dielectric constant

τ_i	Lifetime component i
$\bar{\tau}$	Amplitude-weighted average lifetime
$\chi 2$	Chi-square

List of Abbreviations

(18:0 20:4 PI(4,5)P_2)	1-stearoyl-2-arachidonoyl-*sn*-glycero-3-phospho-(1'-myo-inositol-4',5'-bisphosphate)
(18:1) PI(4,5)P_2	1,2-dioleoyl-*sn*-glycero-3-phospho-(1'-myo-inositol-4',5'-bisphosphate)
(di16:0 PI(4,5)P_2)	1,2-dipalmitoyl-*sn*-glycero-3-phospho-(1'-myo-inositol-4',5'-bisphosphate)
AFM	Atomic force microscopy
Bodipy-PC	2-(4,4-difluoro-5-methyl-4-bora-3a,4a-diaza-s-indacene-3-dodecanoyl)-1-hexadecanoyl-*sn*-glycero-3-phosphocholine
TopFluor-PI(4,5)P_2	1-oleoyl-2-{6-[4-(dipyrromethenebordifluoride)butanoyl]amino}hexanoyl-*sn*-glycero-3-phosphoinositol-4,5-bisphosphate
CF	Carboxyfluorescein
Chol	Cholesterol
DAG	Diacylglycerol
DOPE-Cap-biotin	1,2-dioleoyl-*sn*-glycero-3-phosphoethanolamine-*N*-(cap biotinyl)
DOPE-Rho	1,2-dioleoyl-*sn*-glycero-3-phosphoethanolamine-*N*-(lissamine rhodamine B sulfonyl)
DPPC	1,2-dipalmitoyl-*sn*-glycero-3-phosphocholine
EDTA	Ethylenediamine tetraacetic acid
EtOH	Ethanol
FCS	Fluorescence correlation spectroscopy
FLIM	Fluorescence lifetime imaging microscopy
FRAP	Fluorescence recovery after photobleaching
FRET	Förster resonance energy transfer
GUV	Giant unilamellar vesicle
GPMVS	Giant plasma membrane vesicles
IP3	Inositol trisphosphate
IRF	Instrument response function
Lα	Liquid crystalline phase

Lβ	Tilted gel phase
Lc	Lipid crystalline phase
L_d	Liquid-disordered
L_o	Liquid-ordered
LUV	Large unilamellar vesicle
MeOH	Methanol
MLV	Multilamellar vesicle
NMR	Nuclear magnetic resonance
PA	Phosphatidic acid
PC	Phosphatidylcholine
PE	Phosphatidylethanolamine
PI	Phosphoinositide
PI(4,5)P_2	Phosphatidylinositol (4,5)-bisphosphate
PI(4)P	Phosphatidylinositol (4)-phosphate
PIP4KII	Type II phosphatidylinositol-5-phosphate 4-kinase
PIP5KI	Type I phosphatidylinositol-4-phosphate 5-kinase
PLC	Phospholipase C
PTEN	Phosphatase and tensin homologue on chromosome 10
PS	Phosphatidylserine
PM	Plasma membrane
POPC	1-palmitoyl-2-oleoyl-*sn*-glycero-3-phosphocholine
PS	Phosphatidylserine
SLB	Supported lipid bilayer
SM	Sphingomyelin
STED	Stimulated emission depletion
STORM	Stochastic optical reconstruction microscopy
SUV	Small unilamellar vesicle

TCSPC	Time correlated single photon counting
TORC	Target of rapamycin complex 2
t-PnA	*Trans*-parinaric acid

I. Introduction

1. Biomembranes

Biomembranes are essential components of both prokaryotic and eukaryotic cells, which are tasked with enclosing the cell and separating it from the surrounding environment. They play two important roles: they function as structural barriers and as a cell machine component. While biomembranes provide structure and define the boundaries of the cell, their dynamic biochemical and biophysical properties allow them to regulate traffic and communication to and from the cytosol, organize reaction sequences and promote cellular processes. This makes biological membranes and their predominant components responsible for fundamental processes such as energy transduction, cell-to-cell communication, cell division and maintenance of homeostasis[1].

Biomembrane Structure

The first description of biological membranes as a lipid bilayer was proposed by Gorter and Grendel in 1925[2]. Their work consisted in extracting the lipids from human erythrocytes and depositing them as lipid monolayers. They observed that the area occupied by the monolayer was two times larger than the erythrocyte surface area, which could only be explained by a bilayer lipid structure. Danielli and Davson then proposed that the lipid bilayer must have included proteins adsorbed to the surface of either side of the membrane, in an attempt to explain selective transport of ions and apolar molecules. These two models were the basis for the most recognized biomembrane model- the fluid-mosaic model proposed by Singer and Nicholson in 1972[3]. In this model, the lipids form a two-dimensional viscous matrix in which freely diffusing proteins are adsorbed or embedded either partially or integrally (peripheral and integrated proteins). The membrane would then resemble a mosaic mostly due to the arbitrary feature of the protein-lipid interactions. The most important considerations that were introduced in this model and that were not previously taken into account by Danielli and Davson were: i) the lateral diffusion of both lipids and proteins within the membrane; ii) the lipid motion in the membrane plane at different space and time scales, together with its limited transverse mobility; iii) the presence of proteins with different nature; iv) the lipid phase transitions. All these aspects sum up to an overall fluidity, and most importantly, dynamic lipid bilayer that characterizes the Singer-Nicholson model[4].

Along the years, the fluid mosaic model had to be updated to account for new findings. In revised versions of the model, more attention is given to the mosaic nature of the membrane macrostructure where many protein and lipid components are limited in diffusion. This is of special importance *in vivo* where lipid-lipid, protein-protein and lipid-protein interactions, as well as cell-matrix, cell-cell and intracellular membrane-associated protein and cytoskeletal interactions are important in restraining and modulation the lateral organization of particular membrane components[5].

Eukaryotic membranes present a vast number of distinct membrane lipids, the most common being glycerophospholipids, followed by sterols and sphingolipids.

Glycerophospholipids are composed of two hydrophobic acyl chains (*sn*-1 and *sn*-2 positions) and a phosphate head group (*sn*-3 position) ester-linked to a glycerol backbone. Different classes of glycerophospholipids are organized based on the polar head group ester-linked to the phosphate group[6].

Sphingolipids contain ceramide as their hydrophobic backbone, i.e. a sphingosine molecule amide-linked to a saturated or trans-saturated acyl chain. The polar head group is phosphorylcholine in the case of the most abundant sphingolipid, sphingomyelin (SM), or glycans of varying degree of complexity in the case of glycosphingolipids[7].

Sterols are ubiquitous and apolar membrane components of eukaryotic cell membranes. Their structure is composed by a bulky and inflexible hydrophobic steroid ring linked to a single hydrophilic hydroxyl group. The most abundant sterol in mammalian cells is cholesterol. Basically, sterols rigidify fluid membranes by reducing the flexibility of neighbouring unsaturated acyl chains.

Lipid phase separation

Membrane lipids, in general, are amphiphilic molecules that in the presence of water can show a wide variety of phases with different geometries. Only the lamellar phases will be discussed here.

These states are influenced by temperature, pH, ionic strength, cholesterol content, as well as lipid tail saturation. There are four types of lipid lamellar phases, the crystalline phase (*Lc*), solid-ordered phase, liquid-disordered phase, and lastly liquid-ordered phase.

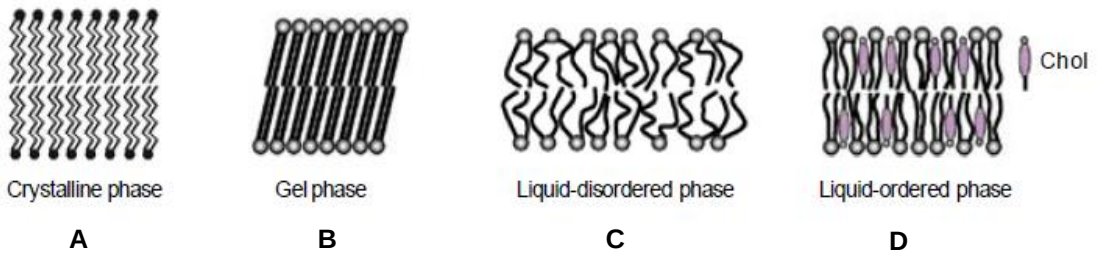

Figure 1. Scheme illustrating the different lamellar phases. Adapted from [8].

The lamellar crystalline (L_c) or subgel phase is formed at low hydration and temperature. The lipid is in a similar packing as in a lipid crystal, with the hydrocarbon chains tightly ordered (figure 1.A)[8]

The solid- ordered phase (L_β), also called gel phase (figure 1.B), present a higher hydration comparative to the lipid crystalline phase. The hydrocarbon lipid chains display an all-*trans* configuration and are elongated at the maximum originating a compact lipid network. Consequently, the lateral diffusion of lipids is reduced. The liquid-disordered (L_d), also known as the fluid phase (figure 1.C) and the liquid-ordered phase (L_o) (figure 1.D), are the most representative of biomembrane lipid phases. In liquid-disordered membranes, the hydration and interfacial area per molecule are increased and the

acyl chains of phospholipids are in a considerable disordered state. Both lateral and rotational diffusion of lipids are favoured in fluid lipid bilayers. In the presence of high sterol concentrations, lipid bilayers can adopt the liquid-ordered phase (L_o) which shares the characteristics of both gel and fluid phases, as it shows considerable acyl chain dynamics while presenting low lateral diffusion rates[8].

Lateral Organization of the plasma membrane

The presence of structured lipid domains, complements the original view of the plasma membrane (PM) by organizing and ordering many different molecular species through specific interactions and creating membrane compartments that support many aspects of membrane and cellular function[9].

In general, lipid domains are defined as lateral membrane heterogeneities generated based on differential lipid–lipid and specific lipid–protein interactions[10]. One of the most discussed types of lipid domains are the so-called lipid rafts,

Rafts are defined as small (10-200 nm wide), highly dynamic, sterol/sphingolipid enriched domains that can compartmentalize cellular processes[11]. From a biophysics point of view, the raft concept in biological membranes is the liquid-liquid phase coexistence that occurs when saturated lipids and sterols condense to form a L_o phase, which is segregated from an unsaturated lipid-rich L_d phase[12]. The basis for this separation resides in specific lipid-lipid, protein-protein and protein-lipid interactions[13]. The lipid raft hypothesis explains the generation of the glycolipid-rich apical membrane of epithelial cells[14], additionally, rafts have been associated with the compartmentalization of some biological process, such as traffic and signalling, endocytosis and exocytosis[15].

The raft concept has been continuously challenged. Although large scale L_d/L_o phase separation can be readily detected in giant plasma membrane vesicles obtained from the PM of eukaryotic cells[16], lipid rafts were never directly observed in the intact PM of living cells, presumably due to their small size, which fall below the resolution of conventional optical microscopy techniques.

The depletion of cholesterol or sphingolipids frequently leads to a loss of membrane organization and protein function, as a consequence of the destruction of lipid rafts.

Another type of domains is the caveola. Caveolae are specialized microdomains of the PM which are defined by their unique morphology. Caveolae have some roles in potocytosis and in signal transduction[17]. The enrichment of signalling molecules in defined microdomains of the PM has led to the suggestion that these domains are crucial to organize and interconnect different signal transduction pathways[18]

Transbilayer organization of the plasma membrane

The plasma membrane of living cells is a highly specialized structure that transmits and controls the information flow between a cell and its environment[19]. In general, membrane are fluid meaning that the bulk proteins and lipids can diffuse laterally in the plane of the membrane[20].

Lipids present continuous bi-directional spontaneous movement between the two leaflets – so-called flip-flop. The spontaneous transmembrane translocation of lipids depends on the nature of the lipid. Uncharged molecules can cross the membrane rapidly due to their lipid solubility in the hydrophobic core of the bilayer, and in these types of molecules the transmembrane translocation is achieved purely by diffusion. On the other hand, lipids with charged or heavily polar head groups show limited translocation rates. In the PM, lipids are asymmetrically arranged between the two leaflets and spontaneous phospholipid flip-flop in the PM act against the formation of this asymmetric distribution. In fact, this asymmetry is only made possible by a lipid-translocation machinery that hydrolyses ATP, with significant energy investment by the cell [21].

The bulk inner leaflet of the PM are composed by PI, phosphatidyletanolamine (PE), phosphatidylserine (PS), phosphatidic acid (PA) and lipids containing polyunsaturated fatty acid (PUFA) residues, while the outer leaflet is most composed of phosphatidylcholine (PC), sphingomyelin (SM) and glycolipids[22].

2. Membrane model systems

Membrane lipid domain formation is often studied in membrane model systems or synthetic membranes, whose composition is usually limited to a few components. Over the years, membrane model systems have been developed that can have their size, geometry and composition tailored by researchers. The most common biomimetic bilayer systems include: supported lipid bilayer (SLBs), small unilamellar vesicles (SUVs), large unilamellar vesicles (LUVs) and giant unilamellar vesicles (GUVs), multilamellar vesicles (MLVs) and lastly giant plasma membrane vesicles (GPMVs).

SLBs are composted by a flat lipid bilayer supported onto a solid surface such as silica. These systems can be prepared easily and are more stable than lipid vesicles [23], however, despite these advantages, the proximity between the lipid bilayer and the solid substate affects the structural and functional properties of the membrane[24].

MLVs are formed when a dry phospholipid film of stacked bilayers deposited on a substrate is hydrated. The resulting MLV suspension contains vesicles that are heterogeneous in size and lamellarity[25].

SUVs and LUVs correspond to a single lipid bilayer with a size below optical resolution. Due to the small size of SUVs (< 50 nm), these vesicles have a very high curvature tension and an asymmetric

total lipid distribution between the two leaflets. Due to this high curvature tension, SUVs are often instable[26].

As the other membrane models, GUVs also provide a well-characterized lipid composition[27]. Additionally, GUVs presenting sizes above 1 µm, allow for the performance of techniques limited by light diffraction such as confocal microscopy and the micromanipulation of individual vesicles[28], which are not possible in smaller vesicles. GUVs provide well-characterized membranes that are free of solid supporting surface, with unconstrained diffusion within the plane of the membrane[29]. The disadvantage of using GUVs is the presence of some vesicle-to-vesicle heterogeneity in lipid composition. GUVs are still a widely used model system due to the already mentioned advantages in imaging and manipulation but also to the fact that their curvature more closely resemble PM of eukaryotic cells.

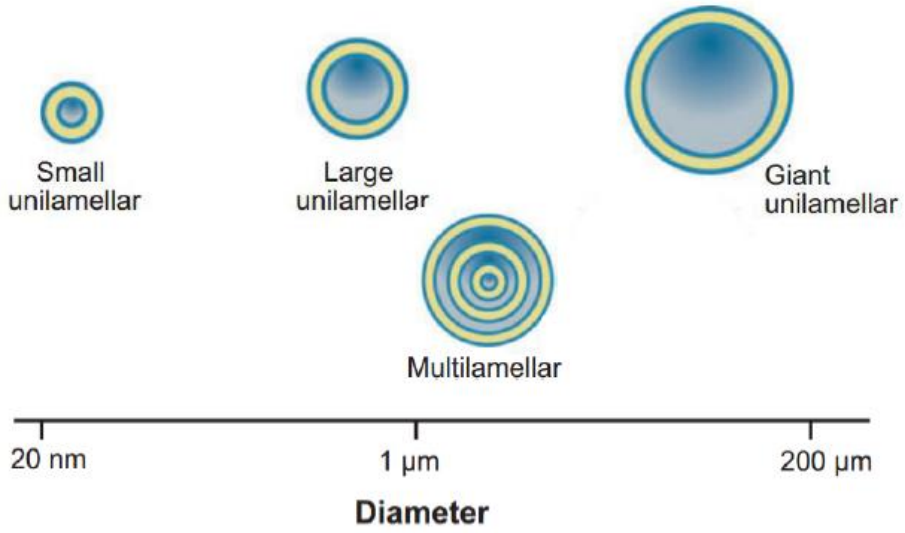

Figure 2. Schematic representation of the most common classification of lipid vesicles, according to their size and lamellarity. Adapted from [68].

3. $PI(4,5)P_2$

Phosphoinositides (PIs) are a small group of glycerophospholipids that comprise around 10-15% of the total membrane phospholipids of eukaryotic cells. These lipids contain a inositol headgroup, containing 5 hydroxylations, three of which, at positions 3,4 and 5, can undergo reversible phosphorylation and desphosphorylation, resulting in seven distinct phosphorylated PI species that account for around 2-3% of the total membrane phospholipids of the eukaryotic cell[30].

Phosphoinositides are not static, and their generation/destruction is under tight spatial and temporal control[31]. PIs are multifaceted molecules due to their involvement in cellular functions such as actin dynamics, membrane trafficking, regulation of transmembrane proteins and signal transduction[32].

$PI(4,5)P_2$ is a member of the phosphoinositide (PI) lipid family [33]. $PI(4,5)P_2$ is the most abundant phosphoinositide in mammalian cells and is found primarily in the inner leaflet of the plasma membrane. Additionally it is also found in endosomes, in the endoplasmic reticulum, and in the nucleus [34]. $PI(4,5)P_2$ can interact, recruit and/or regulate a variety of signalling proteins. It plays a central role in several processes, including cell adhesion and motility[35] vesicle endocytosis and exocytosis and ion channel transport[36].

3.1 $PI(4,5)P_2$ structure, Metabolism and Function

PIs are generally composed by two acyl chains attached to a glycerol backbone, which is connected to an inositol ring by a phosphodiester bond. In mammalians, the two fatty acids are predominantly stearic acid (C18:0) and arachidonic acid (C20:4)[30].Although a net charge of -4 at pH 7.0 is expected, at high ionic strength this charge is actually -3, as a result of the interaction of the lipid with cations.

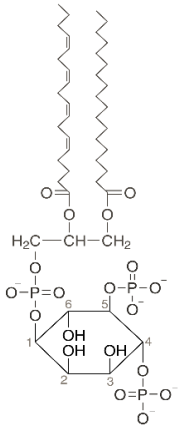

Figure 3. Predominant structure of $PI(4,5)P_2$ in mammalian cell membranes.

$PI(4,5)P_2$ levels are mostly regulated by kinases and phosphatases. Eukaryotic cells have three pathways for $PI(4,5)P_2$ synthesis: two phosphorylations, catalysed by type I phosphatidylinositol-4-phosphate 5-kinase (PIP5KI) and type II phosphatidylinositol-5-phosphate 4-kinase (PIP4KII), and a dephosphorylation catalysed by the protein phosphatase and tensin homologue on chromosome 10 (PTEN). They do not equally contribute to $PI(4,5)P_2$ concentration, and the phosphorylation of PI(4)P by the PIP5KI[37] is responsible for most of $PI(4,5)P_2$ production [38].

The functions of $PI(4,5)P_2$ are associated with the capacity to bind several proteins, targeting them to the PM and controlling their activity in time and space. $PI(4,5)P_2$ plays a key role in the regulation of numerous vital cell functions, from actin cytoskeleton attachment and reorganization to membrane trafficking[39].

Phospholipase C (PLC) also controls $PI(4,5)P_2$ levels and originates metabolites that propagate and amplify cellular signalling. PLC hydrolyses $PI(4,5)P_2$ on the inner leaflet of the plasma membrane into two crucial second messengers, diacylglycerol (DAG) and inositol 1,4,5-trisphosphate (IP3). DAG

controls the activity of various effector proteins containing the conserved C1 domain and acts as the precursor for the synthesis of phosphatidic acid (PA). While, IP3 is a regulator of the cytoplasmic Ca^{2+} concentration[40].

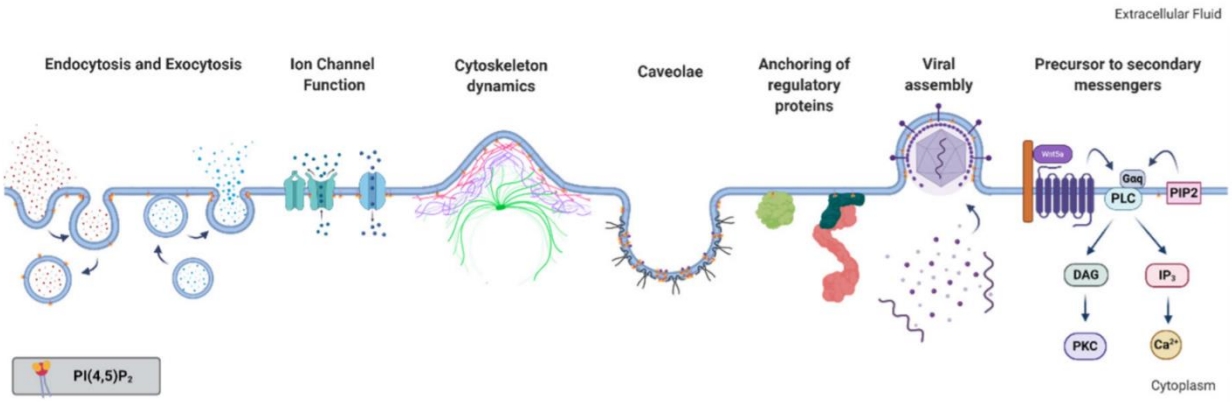

Figure 4. Membrane processes associated with or dependent on phosphatidylinositol 4,5-bisphosphate. Taken from [33].

3.2 $PI(4,5)P_2$ lateral organization

Inside living cells, the levels of $PI(4,5)P_2$-binding proteins are much greater than the $PI(4,5)P_2$ concentration itself [41]. It has been suggested that the regulation of biological processes by $PI(4,5)P_2$ is dependent on the spatiotemporal variation of its concentration, because the regulation of these processes must be accomplished by localized enrichment of $PI(4,5)P_2$ in the PM at a specific sites and timings. It is important that the levels of $PI(4,5)P_2$ must be tightly regulated to avoid fluctuations[33].

$PI(4,5)P_2$ lateral organization in cells has been studied through several techniques such as Fluorescence correlation spectroscopy (FCS), Fluorescence recovery after photobleaching (FRAP) and Atomic force microscopy (AFM). In FCS experiments carried out in Rat1 fibroblasts and HEK cells, researchers microinjected micelles of fluorescent labelled-$PI(4,5)P_2$ into cells and showed that the diffusion coefficient (D) of $PI(4,5)P_2$ in the PM of these cells is lower than expected for free phospholipids. Using Stimulated emission depletion (STED) microscopy[42] and Stochastic optical reconstruction microscopy (STORM)[43] imaging techniques, studies in PC12 cells shown that $PI(4,5)P_2$ is highly enriched in nanometer-sized membrane domains within the PM, specific to this cellular model.

$PI(4,5)P_2$ interactions with other cellular binding partners could alternatively explain the observed lateral organization. Interactions with proteins, divalent cations, cholesterol, and the cytoskeleton are the ones most likely to have an impact [33].

One example is that proteins can act as reversible buffer, binding the $PI(4,5)P_2$ present and releasing it locally in response to specific signals. The sequestering by proteins can be achieved through specific and also nonspecific electrostatic interaction with $PI(4,5)P_2$[33].

4. Ca^{2+} induced $PI(4,5)P_2$ clustering

$PI(4,5)P_2$ is able to establish strong electrostatic interactions between its negatively charged headgroup and positively charged proteins or divalent cations. In the cellular context, calcium (Ca^{2+}) and magnesium (Mg^{2+}) stand out as $PI(4,5)P_2$ binding partners [33]. Calcium has an important role in signal transduction and as a second messenger in cells. Its level are tightly controlled and maintained at low concentrations in the cytosol, with resting intracellular levels at around 100 nM [44]. On the other hand, free magnesium levels are well buffered in a narrow millimolar range between 0.25 mM and 1 mM [45,46] and are thus kept at a much higher concentrations than those of calcium. Both divalent cations have been shown to bind to $PI(4,5)P_2$ and influence its lateral organization [33], albeit calcium does do with much greater affinity. Indeed, there are several experimental results that confirm that magnesium is weaker than calcium in inducing $PI(4,5)P_2$ clusters[47,48]. In these clusters, divalent cations associate with more than one $PI(4,5)P_2$ molecule, stabilizing a network of mixed cation-$PI(4,5)P_2$ molecules within clusters.

Divalent cation-mediated clustering leads to the formation of specific sites in the membrane which are highly enriched in $PI(4,5)P_2$, while depleting the rest of the membrane. These cation-induced effects can influence not only $PI(4,5)P_2$ lateral organization but also the way $PI(4,5)P_2$ interacts with proteins, by modulating their localization in the PM, their target recognition and binding affinity to $PI(4,5)P_2$, and even further interactions with other proteins[49]. $PI(4,5)P_2$ itself is homogeneously distributed in liquid disordered membranes in the absence of divalent ions. The addition of Ca^{2+} was shown to induce $PI(4,5)P_2$ clustering at high and non-physiological concentrations in lipid monolayers LUVs and GUVs[50]. Some evidences suggested that divalent cations can not only reduce the electrostatic repulsion between the anionic PIP_2 head groups but also act as bridges between two adjacent lipids, where macromolecular aggregates of PIP_2 were induced by Ca^{2+}[41]

Furthermore, in membranes containing cholesterol, Ca^{2+} seems to favour partition of $PI(4,5)P_2$ molecules to raft-like domains, where clustering seems to be more efficient. Ca^{2+} may even potentiate protein anchoring in cholesterol-enriched domains, by increasing $PI(4,5)P_2$ density in these microdomains[50].

5. $PI(4,5)P_2$-protein Interaction

Interactions of proteins with lipids can drive enrichment of the bilayer around the protein in these lipids and deprivation in others, creating local heterogeneities that can potentially extend to several lipid shells around the protein [51].

Phosphoinositides affect cellular functions by interacting with molecules that reside in the membrane. Several signalling molecules are recruited to the membrane through interaction with PIs via inositide-binding protein modules[52].

Binding of $PI(4,5)P_2$ to lipid binding domains can serve to activate proteins as well as merely anchoring them to the plasma membrane. $PI(4,5)P_2$ is able to recruit specific proteins to particular sites of the PM at given times, thus controlling a variety of cell processes in time and space. These lipid-

protein interactions play a key role in the regulation of numerous vital cell functions, from actin cytoskeleton attachment and reorganization to membrane trafficking[39]

6. PI(4,5)P_2 as a lipid sensor for membrane tension

Another property of lipid membranes that has not been introduced here yet is membrane tension. In a lipid bilayer, lipid molecules interact in such a way as to maximize interactions between their hydrophobic tails and between their hydrophilic headgroups. This results in a specific average area per lipid molecule or lipid packing density that allows for moderate in-plane stretching and compression before rupture of the bilayer structure (Fig. 5)[53]. Membrane tension is the force necessary to stretch the membrane. Increasing the lipid spacing by osmotic swelling of a vesicle or cell, for example, is strongly resisted, and leads to rupture of the bilayer when the membrane is strained slightly above its normal packing density[53]. In-plane compression is also resisted, but vesicles and cells can adjust to this through changes in curvature of the membrane.

Plasma membrane tension is used to control multiple cellular events. Cells need to maintain homeostasis of PM tension by sensing the change of tension and modulating their membrane area or cytoskeletal attachment via endocytosis, exocytosis, membrane invagination. Until recently, known sensors of PM tension were generally transmembrane proteins or peripheral membrane proteins, including stretch-activated ion channels, curvature-sensing proteins or membrane interacting proteins. Membrane–cytoskeleton and osmotic pressure can also contribute to PM tension[54].

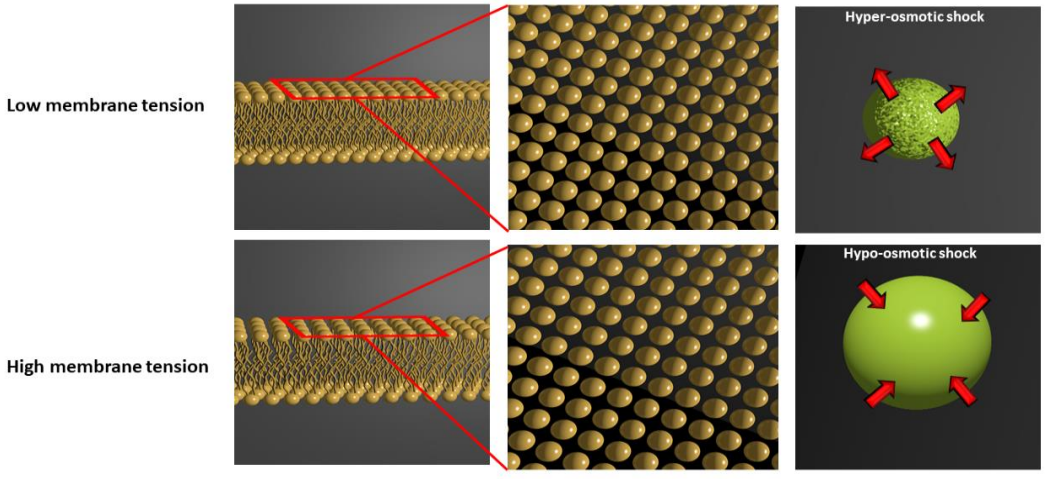

Figure 5. Changes in lipid organization associated with low or high membrane tension, produced respectively by hyper- and hypo-osmotic shocks.

The target of rapamycin complex 2 (TORC2) plays a vital role in maintaining the homeostasis of the PM tension. TORC2 is recruited to the PM through binding to PI(4,5)P_2[55]. Recent studies have shown

that a decrease in the membrane tension triggers PI(4,5)P_2 phase separation into membrane invaginations and leads to co-clustering of TORC2 with PI(4,5)P_2 within these areas, with concomitant inactivation of TORC2 (Figure 6) [55]**.** These areas were labelled as PI(4,5)P_2 enriched structures (PES) and were immediately disassembled upon membrane stretching through osmotic shock [55]**.** TORC2 inactivation through this mechanism was required for recovery of yeast cells from hyperosmotic shock [55]. PI(4,5)P_2 was shown to be necessary for the formation of PES invaginations and sequestering of inactive TORC2 to PES appeared to result from PI(4,5)P_2 phase separation induced directly by a decrease in PM tension. This sequestering was energy independent, suggesting spontaneous segregation. Additionally, the lipid membrane within PES is shown to have higher membrane order than the rest of membrane, suggesting that such areas correspond to liquid-ordered domains [56].

Strikingly, the results regarding the relationship between PI(4,5)P_2 distribution and membrane tension presented the interesting possibility that PI(4,5)P_2 is the primary molecular sensor of decreased PM tension, with further activation/deactivation of PM membrane tension sensors acting just as responses to this initial and possibly spontaneous event [55].

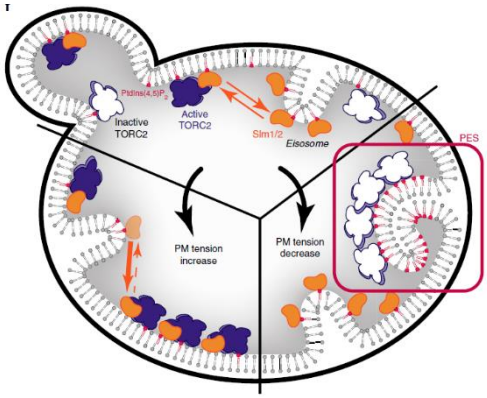

Figure 6. Increased and decreased PM tension are sensed through different mechanisms by TORC2. Decreased PM tension triggers a spontaneous, energy-independent PI(4,5)P_2 phase separation into invaginated membrane. Taken from[55].

7. Role of PI(4,5)P_2 in cellular thermal adaptation.

The environmental temperature produces a change in membrane lipid composition, in the case of a lower temperature the membrane composition is characterized by an increased abundance of phospholipids with shorter chain lengths and/or unsaturated fatty acids[57]. PI(4,5)P_2 is an important regulator of lipid metabolism in response to thermal stress. Thus, a drop in temperature reduces PI(4,5)P_2 levels and so the activity of some essential signalling effector in response to cold[57].

Importantly, chaotropic agents (e.g., salts, trehalose, urea, temperature) that disrupt water structure and the ability of water to mediate intermolecular hydrogen bonding also induce an increase in PI(4,5)P_2 surface area [58]. In fact, when the temperature went from 17 to 34°C, the area per PI(4,5)P_2 molecule increased by 50%, while that of other lipids only did by 10%[58], reflecting the expected scaling

of area with temperature. The dramatic increase in surface area with temperature was hypothesized to be associated with a disruption of the hydrogen boding network as temperature increases. In this case, the structure of $PI(4,5)P_2$ clusters is expected to show considerable differences at different temperatures. Studies on $PI(4,5)P_2$ clustering have overwhelmingly focused on the behaviour of these molecules at room temperature. In Sarmento et al (2017)[50], experiments on $PI(4,5)P_2$ clustering in POPC:sphingomyelin:cholesterol membranes were carried out at both 25 and 37 °C. Significant differences in $PI(4,5)P_2$ clustering were observed then, but this was rationalized as stemming exclusively from differences in membrane phase structure and order. In this way, the direct impact of temperature on $PI(4,5)P_2$ clustering remains largely unexplored. When this question is solved, the issue of whether the $PI(4,5)P_2$ monomer/cluster duality has an impact on PI(4,5)P2 signalling in response to cellular thermal adaptation can be tackled.

8. Impact of cholesterol on $PI(4,5)P_2$ nanodomais

Cholesterol is an important membrane component in many of membrane processes. In general, cholesterol decreases membrane fluidity by increasing lipid packing. $PI(4,5)P_2$, was show to favourably partition into the liquid disordered phase (cholesterol depleted) of the monolayer due to its large negatively charged headgroup and highly unsaturated acyl chain[33]. Surprisingly, this preference was largely disrupted in the presence of divalent cations, which at very high concentrations even induced a shift in partition to a moderate preference for liquid-ordered phase[50].More recently, saturated $PI(4,5)P_2$ species were shown to generate solid gel-phase lipid domains in the presence of calcium (Borges-Araújo, in press[59]). The formation of such structures in the PM is bound to have dramatic consequences to cell health as the solid gel phase is generally associated with cell aging and death. Due to dramatically reduced dynamics in these structures, it is likely that $PI(4,5)P_2$ molecules in these gel domains are unable to interact effectively with $PI(4,5)P_2$-binding proteins, rendering then as inactive for signalling purposes.

Gel domains by high melting temperature lipids of other classes are seldomly observed in the PM of healthy cells. The main reason for this is the inhibitory effect of sterols in the formation of lipid gel phases as sterols show preferential interaction with high melting temperature lipids, leading to the formation of liquid ordered domains instead of solid gel phases[60,61]. In fact, the high cholesterol concentration at the PM of animal cells shifts the threshold for gel phase formation to a concentration of gel triggering lipids that is considerably above their natural abundance. This effect is of critical importance for cell viability. However, in the case of saturated $PI(4,5)P_2$, gel phase formation is mostly triggered by segregation of the lipids due to headgroup interactions, and not due to acyl-chain packing preferences as seen for other lipid classes. In this way, it is not clear if cholesterol could prevent the formation of such phases. If not, the prevalence of the polyunsaturated canonical $PI(4,5)P_2$ specie, which evolution favoured, could have risen as a mechanism to prevent the formation of solid $PI(4,5)P_2$ domains. Recently, the polyunsaturated canonical $PI(4,5)P_2$ specie inhibited was also shown to inhibit the formation of gel phase by the saturated $PI(4,5)P_2$, supporting this hypothesis[59].

II. Materials and Methods

1. Chemicals

1.1 Reagent

1-Palmitoyl-2-oleoyl-*sn*-glicero-3-phosphocholine (POPC), 1,2-dioleoyl-*sn*-glycero-3-phospho-(1'-myo-inositol-4',5'-bisphosphate) (di18:1PI(4,5)P2), 1-stearoyl-2-arachidonoyl-*sn*-glycero-3-phospho-(1'-myo-inositol-4',5'-bisphosphate)(18:020:4PI(4,5)P_2),1-oleoyl-2-{6-[4 (dipyrromethene borondifluoride)butanoyl]amino}hexanoyl-*sn*-glycero-3-phosphoinositol-4,5-bisphosphate (TopFluor PI(4,5)P_2), and 1,2-dioleoyl-*sn*-glycero-3- phosphoethanolamine-N-(cap biotinyl) (DOPE-Cap-biotin), 2-(4,4-difluoro-5-methyl-4-bora-3a,4a-diaza-s-indacene-3-dodecanoyl)-1-hexadecanoyl-*sn*-glycero-3-phosphocholine (BODIPY-PC). All lipids were purchased from Avanti Polar Lipids (Alabaster, AL, USA).1,2-Dipalmitoyl-*sn*-glycero-3-phospho-(1'-myo-inositol-4',5'-bisphosphate) (di16:0 PI(4,5)P_2) was from Echelon Biosciences (Salt Lake City, UT, USA). Lipid stock solutions were prepared in chloroform, except for the phosphoinositides, which were prepared in chloroform: methanol (MeOH) 2:1(v/v). Both solvents were obtained from Merck (Darmstadt, Germany) and were of spectroscopic grade. Ethanol (EtOH), NaCl, Sucrose, EDTA, glucose and $CaCl_2$ were from Sigma-Aldrich (St. Louis, MO, USA). Trans-parinaric acid, DOPE-Rhodamine and Fluo-5N were from Molecular Probes, Invitrogen (Eugene, OR, USA). Avidin egg white and cholesterol (chol) were from Sigma Chemical Co. (St. Louis, MO). All organic solvents were UVASOL grade from Merck Millipore (Darmstadt, Germany).

1.2 Fluorescent Probes

Fluorescent probes were quantified spectrophotometrically using absorption coefficients obtained from literature (table 1).

Table 1. Probe spectral properties. Absorption coefficient, excitation/absorbance and emission maximum wavelengths are shown as well as the storage solvents for each probe.

Probe	ε_{max} ($M^{-1}cm^{-1}$)	$\lambda^{max\ abs/exc}$ (nm)	$\lambda^{max\ em}$ (nm)	Solvent	Reference
Fluor-5N	72 000	495	515	Water	[62]
TopFluor-PI(4,5)P_2	80 000	500	504	Chloroform:Methanol (2:1)	[63]
Flipper-TR	16 600	480	600	DMSO	[64]
BODIPY-PC	86 000	514	516	Chloroform	[63]
DOPE-Rhodamine	95 000	540	566	Chloroform	[65]
t-PNA	91 000	299	320	Ethanol	[66]

2. Model membrane systems

1.1 Large unilamellar vesicles

The lipid mixtures were prepared from phospholipid stock solutions and dried to lipid films under a nitrogen flux. Lipid films were kept in vacuum for 3 hours to remove the last traces of solvent. Samples were hydrated using a solution of 150 mM NaCl, pH=7.4. Freeze-thaw cycles were performed, using liquid nitrogen and a water bath typically set to 60 ºC. The thawing temperature used was always higher than the melting temperature of the lipid with the highest melting temperature in the mixture, to re-equilibrate and homogenize the samples. LUVs were obtained by extrusion at room temperature, using an Avanti Mini-Extruder (Alabaster, AL) and 100nm pore size polycarbonate membranes (Whatman, USA). Typically, at least 21 passages through the extruder were performed.

2.2 Giant unilamellar vesicles

GUVs were obtained by gel-assisted formation and by electroformation in Pt wires, both based on previously described methods[67,68].

In the case of gel-assisted vesicle formation, the lipid mixtures were prepared, from stock solutions, in chloroform to a final concentration of 1.5 mM. These were composed of 95% POPC and 5% PI(4,5)P2. A solution of 5% (w/w) polyvinyl alcohol (PVA) MW ~145 000 and 200 mM of sucrose was spread in a µ-slide chamber from Ibidi (Munich, Germany) and left to dry for 15 minutes at 50 ºC. The desired lipid mixture was then spread on the PVA surface. The solvent was evaporated for 15 minutes under vacuum. After evaporation of the solvent, the appropriate solution with 200 mM sucrose was added, allowing for GUV formation for 60 minutes at room temperature. After the formation, GUVs were transferred to a µ-slide chamber with the appropriate coating.

For the electroformation, lipid solutions were prepared in chloroform (from lipid stock solutions) in a probe/lipid ratio of 1/500 (mol:mol) for Rho-DOPE, and 1/200 for TF-PI(4,5)P_2. After removal of the solvent, electroformation was performed in 1mL of a 200mM sucrose solution. After formation, GUVs were transferred to a µ-Slide from Ibidi (Munich, Germany) coated with avidin, and a 200 mM glucose solution was also added to the wells in order to increase GUV deposition and immobilization rate.

For immobilization of GUVs in the coverslip surface for imaging in the fluorescence microscope, a small concentration of biotinylated phospholipid (DOPE-cap-biotin) was added to the lipid mixture at a 1:10^6 molar ratio of biotinylated lipid to total lipid. Slides from Ibidi (Munich, Germany) were passively coated with avidin by incubation for 1 hour with 200 µL of a concentrated (0.5mg/ml) solution of the protein, followed by extensive rinsing with MilliQ water and sample buffer. Sucrose containing GUV solutions were transferred to these slides and glucose solution was then added to the vesicles in order to create a density difference and promote sedimentation of vesicles in the bottom coverslip, so that a greater number of vesicles can be imaged. Before measurements, slides were left immobile in the dark during 20 min, allowing time for GUVs to attach to the surface.

2.3 Lipid quantification

Lipid stock solutions were prepared in chloroform, except for all PIPs and TopFluor-PIPs (TF-PIPs) that were prepared in chloroform/methanol (2:1 v/v). The concentration of POPC, PSM, DOPE-Cap-biotin and PI(4,5)P_2 stock solutions were determined using an inorganic phosphate colorimetric quantification method. This method is based on the determination of inorganic phosphate obtained after acid hydrolysis of phospholipids with perchloric acid (Merck) at 200ºC. The released phosphate reacts with ammonium heptamolibdate to form phosphomolybdic acid, which in turn is reduced by ascorbic acid, yielding a blue compound detectable spectrophotometrically at 815 nm. Cholesterol concentration was determined by gravimetry (Mettler Toledo UMT2).

2.4 Calcium quantification

Buffer calcium concentration in the micromolar range were determined using a fluorescent calcium indicator, Fluo-5N pentapotassium salt. The quantification of free Ca^{2+} is then possible using fluorescence measurements.

Response calibration was carried out by measuring the fluorescence intensity of the probe in buffer with a saturating amount of free Ca^{2+} (10 mM of $CaCl_2$) and in buffer containing no free Ca^{2+} (5 mM of EDTA). The calibration samples were prepared with a Fluo-5N concentration of 0.5µM. Using the same sensor concentration and through measurement of fluorescence intensity in the different buffers used in this work, the following equation could then be used to quantify free Ca^{2+} concentrations:

$$\left[\boldsymbol{Ca^{2+}}\right] = \boldsymbol{K_d}\frac{[\boldsymbol{I - Imin}]}{[\boldsymbol{Imax - I}]} \quad (1)$$

Where $Imin$ is the fluorescence intensity of the indicator in the absence of calcium, $Imax$ is the fluorescence of the calcium saturated indicator, I is the experimental fluorescence intensity and Kd is the calcium dissociation constant of Fluo-5N (Kd =90 µM).

Fluo-5N was excited using 480 nm radiation and fluorescence emission collected from 490 to 600 nm.

2.5 Dynamic light scattering and zeta-potential

Dynamic light scattering measurements of liposomes were carried out in a Malvern Zetasizer Nano ZS (Malvern, UK) equipped with a 4 mW He–Ne solid-state laser operating at 633 nm and backscattered light was detected at 173°. Liposomes were measured in 10 mM HEPES buffer (150 mM

NaCl, pH=7.4) at a lipid concentration of 200 µM. Zeta-potential (F) of liposomes were determined at 25ºC from the mean of 3 measurements (100 runs each), in the presence of different calcium concentrations, using DTS 1060 disposable folded capillary zeta cells with gold electrodes (Malvern, UK), after 30 seconds of equilibration time. All the results were processed using the instrument Malvern's DTS software.

3. Absorption and fluorescent measurements

3.1 UV visible spectroscopy

UV-visible absorption measurements were performed using a JASCO V-660 UV-VIS spectrophotometer (JASCO, Tokyo, Japan), at room temperature, using a bandwidth and sampling interval of 1 nm. For the spectrophotometric quantification, quartz cuvettes (Hellma Analytics) with a path length of 1 or 0.5 cm were used.

3.2 Steady-state fluorescence anisotropy

Fluorescence measurements were carried out in a JASCO FP-8500 spectrofluorimeter (JASCO, Tokyo, Japan) equipped with a peltier temperature controller and Polarizers. Both fluorescence intensity and fluorescence anisotropy measurements were carried out in quartz cuvettes (Hellma Analytics) having a path length of 0.5 cm. Fluorescence intensity values of TF-PI(4,5)P_2 were recovered from the integration of fluorescence emission spectra obtained with an excitation of 460 nm. Fluorescence anisotropy values were obtained using 460 and 510 nm for excitation and emission wavelengths, respectively.

Fluorescence anisotropy measurements are based on the principle of photoselective excitation of fluorophores by polarized light. Fluorophores preferentially absorb photons whose electric vectors are aligned parallel to the transition moment of the fluorophore. The transition moment has a defined orientation with respect to the molecular axis. If the excitation light is linearly polarized, then fluorophore excitation occurs preferentially if the electric field of the excitation light is oriented parallel to the absorption transition dipole moment, while fluorescence light polarization is related to the emission transition dipole moment. Fluorescence anisotropy, by quantifying the extent of depolarization of emission fluorescence after excitation with polarized light, reveals the average angular displacement of the fluorophore that occurs during the fluorophore excited state. Fluorescence anisotropy has been used to measure binding constants of kinetic reactions, folding dynamics and membrane viscosity. Additional causes of fluorescence depolarization are homoFRET events and changes in orientation of the transition moment of the excited-state relative to the ground-state.

The extent of emission polarization is described in terms of the anisotropy steady-state ($< r >$) and can be calculated by the following equation (2):

$$< r >= \frac{I_{VV} - GI_{VH}}{I_{VV} + 2GI_{VH}} \quad (2)$$

Where I_{vv} and I_{VH} are the steady-state vertical and horizontal components of fluorescence emission, respectively, with vertically polarized excitation. The components with excitation horizontal to the emission axis, I_{HV} and I_{HH}, are used to calculate the factor G, present on equation (3):

$$G = \frac{I_{HV}}{I_{HH}} \quad (3)$$

The *G* factor is the ratio of the system's different sensitivities for vertically and horizontally polarized light and is used to correct fluorescence anisotropy measurements.

3.3 FRET and HomoFRET

Förster resonance energy transfer (FRET) is a non-radiative energy transfer mechanism, where a donor molecule in the excited state transfers energy to an acceptor molecule in the ground state through a long range resonant dipole-dipole coupling mechanism.

For FRET to occur, three crucial physical conditions must be met: 1) donor emission spectrum must overlap with the acceptor absorption spectrum; 2) the donor and acceptor molecules must be in close proximity (between 1 and 10 nm); 3) the donor emission dipole moment and acceptor absorption dipole moment must be properly oriented.

FRET can occur between identical molecules, and in this case, it is called homoFRET. HomoFRET normally occurs between fluorophores that display small Stokes shifts and the donor and the acceptor are spectroscopically indistinguishable. Therefore, in this case, intensity ratios and lifetime measurements cannot be used to quantify the energy transfer efficiency. Fluorescence anisotropy is the only method for detecting and quantifying homoFRET, as FRET events lead to light depolarization.

3.3 Confocal fluorescence microscopy

Confocal laser scanning fluorescence microscopy measurements were performed on a Leica TCS SP5 (Leica Microsystems CMS GmbH, Manheim, Germany) inverted confocal microscope (DMI600). A 63x apochromatic water immersion objective with a NA 1.2 (Zeiss, Jena Germany) was

used for all measurements, and an Argon laser was used for excitation. All analysis of confocal imaging data was carried out using ImageJ.

3.4 Fluorescence lifetime imaging microscopy (FLIM)

Fluorescence lifetime imaging microscopy (FLIM) measurements were performed through time correlated single photon counting (TCSPC) using the same setup of confocal microscopy, coupled to a multiphoton Titanium: Sapphire laser (Spectra- Physics Mai Tai BB, Darmstadt, Germany, 710–990 nm, 100 femtosecond pulses, 80 MHz) as an excitation source. A photomultiplier tube was coupled to the X-port of the microscope and the emitted photons were processed by an SPC board that addresses simultaneously the (x, y) location of the collected photons (Becker and Hickl, GmbH, PMC-100-4 SPC-830). The laser power was adjusted to give an average photon counting rate higher than 5x104 photons per s and images were acquired for 60 seconds to achieve reasonable photon statistics.

The excitation wavelength was set to 800 nm and emission light was selected using a dichroic beam splitter with an excitation SP700 short-pass filter and an emission 647/75 bandpass filter inserted for Flipper-TR in front of the photomultiplier, and for TF-PI(4,5)P_2 was used dichroic beam splitter with an excitation SP700 short-pass. Images were acquired using a Becker and Hickl SPC 830 module. Fluorescence lifetimes were obtained by analysing the fluorescence decays through a least square iterative re-convolution of decay functions with the instrument response function (IRF) using the software SPC Image (Becker and Hickl, Berlin, Germany).

3.5 Time-resolved fluorescence spectroscopy

Fluorescence decay measurements were carried out using the time-correlated single-photon timing (TCSPT) technique, as described elsewhere [69]. The emission wavelength was selected by a Jobin Yvon HR320 monochromator (Horiba Jobin Yvon, Kyoto, Japan). 0.5 × 0.5 cm^2 quartz cuvettes from Hellma were used. Blank decays were acquired, and photon counts were negligible. The fluorescence intensity decays were described by a sum of exponentials:

$$\boldsymbol{i(t) = \sum_i \alpha_i \exp\left(-\frac{t}{\tau_i}\right)} \tag{4}$$

where α_i is the normalized amplitude and τ_i is the i^{th} lifetime component. The amplitude-weighted average lifetime is defined as:

$$\boldsymbol{\bar{\tau} = \sum_i \alpha_i \tau_i} \tag{5}$$

Data analysis was performed with the TRFA software (Scientific Software Technologies Center, Minsk, Belarus), based on Levenberg–Marquardt nonlinear least-squares fitting. The goodness of the fit was judged from the experimental chi-squared (χ^2), weighted residuals and autocorrelation plot. In every analysis, χ^2 was below 1.3 and both the residuals and the autocorrelation were randomly distributed around zero.

III. Results

1 Electrophoretic Light Scattering

In order to confirm interaction of calcium with PI(4,5)P_2 within liposomes, the surface charge of liposomes containing PI(4,5)P_2 was evaluated in the presence of different calcium concentrations using electrophoretic light scattering measurements. We prepared LUVs containing 5% PI(4,5)P_2 and 95% of POPC in 10, 50 and 100 µM Ca^{2+} buffer, and also in the absence of calcium (5 mM EDTA). The total concentration of lipids in this experiment was 200 µM.

The zeta potential is defined as the potential at the hydrodynamic shear boundary and reflects the surface charge around the particle. It is calculated from the velocity or electrophoretic mobility using Henry equation (Eq. 5)

$$U_e = \frac{2\,\varepsilon\, z\, f(ka)}{3\,\eta} \qquad (5)$$

where U_e is the electrophoretic mobility, ε is the dielectric constant, z is the zeta potential, η is the absolute zero-shear viscosity of the medium. is the Henry function, while k and a refer to the Debye length and radius of the particle, respectively [70].

For PI(4,5)P_2 at pH 7.0, the phosphomonoester proton is dissociated, while the two phosphodiesters present one proton fully dissociated each and one proton remaining is shared by both groups [71]. As such, the net charge is -4, and the lipid is expected to confer anionic charge to the surface of the liposomes where it is incorporated. The values of zeta potential recovered for liposomes containing PI(4,5)P_2 were less negative than expected, considering the concentration (5%) of the highly anionic lipid. Still, it is possible to notice that liposomes with PI(4,5)P_2 at a temperature of 25ºC (Figure 7) have considerably more negative charge when compared to the zwitterionic POPC at the same temperature. In addition, we see that this difference decreases with increasing calcium concentration, due to association of Ca^{2+} with the membrane and PI(4,5)P_2 charge neutralization.

These results clearly demonstrate calcium association to the lipid membrane containing PI(4,5)P_2. At this lipid concentration, 100 µM of $CaCl_2$ is nearly sufficient for complete surface charge neutralization, suggesting that PI(4,5)P_2 are almost saturated with Ca^{2+} ions.

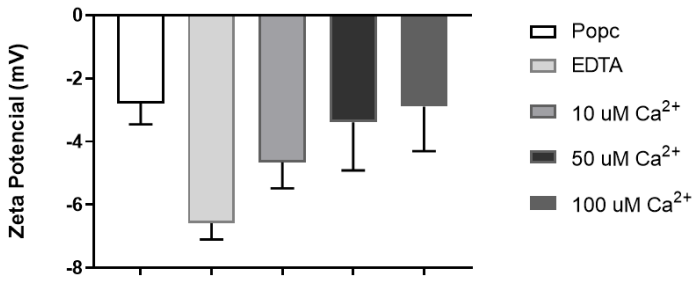

Figure 7. Zeta potential at 25ºC. The results represent the mean of 3 measurements (N=6), 100 runs each with a equilibration time of 30 seconds in the presence of different calcium concentrations.

2 Impact of temperature on calcium-dependent PI(4,5)P_2 clustering

Temperature is a strong modulator of lipid membrane structure and dynamics. In the case of calcium-induced PI(4,5)P_2 clustering, the importance of temperature for the formation of such structures is still unclear. In order to clarify this issue, fluorescence spectroscopy measurements were carried out with the fluorescent analogue TF-PI(4,5)P_2.

TF-PI(4,5)P_2 was previously shown to incorporate within Ca^{2+}-induced clusters of PI(4,5)P_2[50,72] , and clustering of PI(4,5)P_2 can be detected by either fluorescence self-quenching or homo-FRET between fluorescent analogues of PI(4,5)P_2 (TF-PI(4,5)P_2)[50,72]. The former is readily detected from changes in fluorescence intensity of the analogue, while the latter has no impact on fluorescence intensity. In order to detect homo-FRET changes, only fluorescence polarization studies are useful, since FRET events inevitably leads to depolarization of fluorescence emission. The extent of FRET efficiency (E) can thus be evaluated from changes in fluorescence anisotropy.

In order to test the effect of temperature on calcium-induced PI(4,5)P_2 clustering, we prepared LUVs containing a mixture of POPC:PI(4,5)P_2:TF-PI(4,5)P_2 at a 97.4:2.5:0.1 molar ratio. Different calcium concentrations were also tested, namely 10, 50 and 100 μM Ca^{2+} buffer.

In order to probe the behaviour of monomeric PI(4,5)P_2, EDTA was added as a chelating agent, since the chelating agent impedes the formation of any divalent cation-dependent cluster. This is necessary, given the inevitable presence of metal residues even in heavily purified water. In these samples, the fluorescence intensity of the TF-PI(4,5)P_2 monomer decrease, as temperatures increase (Figure 8.A). This is also evident in the presence of calcium and reflects the general decrease with temperature of the quantum yield of the 4,4-difluoro-4-bora-3a,4a-diaza-s-indacene fluorophore. This is to be expected as non-radiative processes related to thermal agitation (collisions with solvent molecules, intramolecular vibrations and rotations, etc.) are more efficient at higher temperatures.

At a given temperature, fluorescence self-quenching within the calcium-induced PI(4,5)P_2 and TF-PI(4,5)P_2 aggregates leads to further decreases in fluorescence intensity of TF-PI(4,5)P_2. This decrease is progressive as calcium concentration increases (Figure 8.A) and reflects the increase of the fraction of PI(4,5)P_2 fluorescent analogue within aggregates, as more calcium binds the membrane.

In this way, at a given temperature, the fluorescence intensity is defined by the ratio of monomeric TF-PI(4,5)P_2/clustered TF-PI(4,5)P_2. Most of the fluorescence self-quenching is observed already at 10 μM Ca^{2+}, and more moderate changes are observed as calcium levels increase above this value, suggesting that PI(4,5)P_2 is already close to full incorporation in clusters at these calcium levels.

Recent results demonstrated that the clustered PI(4,5)P_2 exhibits significantly increased molecular order than the monomer[59]. This is also evident from the normalized fluorescence intensity (Figure 8.B), which shows that the monomeric TF-PI(4,5)P_2 is more sensitive to an increase in thermal associated dynamics than the clustered molecules.

In case thermal associated dynamics reduced the stability of calcium-dependent PI(4,5)P_2 clusters, a progressive shift of the fluorescence intensity towards the values observed for the monomer,

was to be expected at higher temperatures. In this case, the fluorescence self-quenching due to clustering would be progressively alleviated, particularly at low calcium concentrations. On the contrary, normalized fluorescence intensity values of the lipid analogue when calcium is present, show almost no variation with calcium concentration (Figure 8.B). This suggests that there are no variations in the percentage of TF-PI(4,5)P_2 aggregated with temperature, and for the whole range of temperatures analysed, PI(4,5)P_2 remains almost fully incorporated within clusters, even in the low range of calcium levels (10 μM).

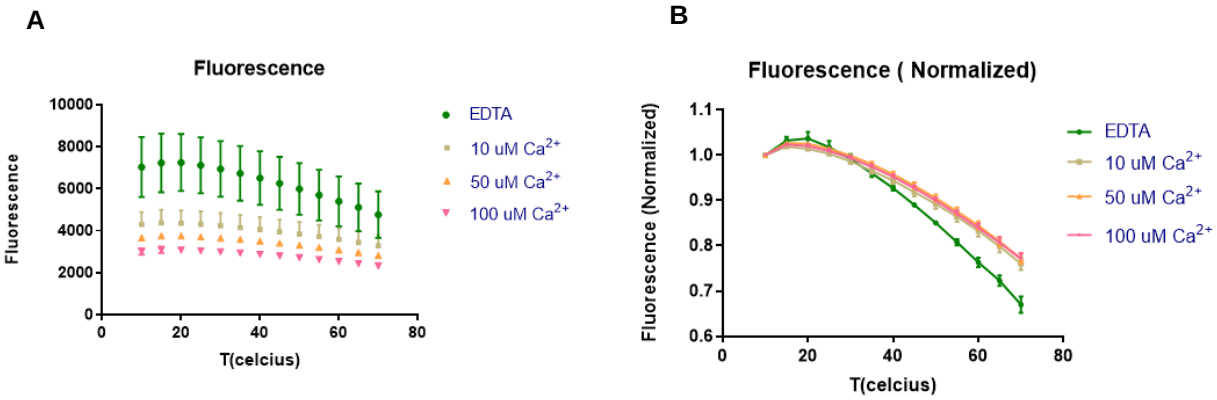

Figure 8. Impact of temperature on TF-PI(4,5)P_2 self-quenching. A- Fluorescence; B- Fluorescence normalized to maximum value at each calcium concentration. Fluorescence intensity values of TF-PI(4,5)P_2 were obtained with an excitation wavelength of 460 nm and emission wavelength of 510 nm. LUVs contained a mixture of POPC:PI(4,5)P_2:TF-PI(4,5)P_2 at a 97.4:2.5:0.1 molar ratio in the presence of different calcium concentrations (10, 50 and 100 μM Ca^{2+}). All measurements were taken at a range of temperatures between 10 ºC-70 ºC.

In order to confirm this observation, the temperature dependence of the fluorescence anisotropy of TF-PI(4,5)P_2 was also evaluated. TF-PI(4,5)P_2 fluorescence anisotropy (<*r*>) values reflect fluorescence depolarization and in the absence of homoFRET would depend mostly on the dynamics of the system, which is expected to increase with temperature as a result of greater lipid mobility in the membrane during the excited-state of the fluorophore. In this case, temperature increases are expected to induce a considerable decrease in fluorescence anisotropy of TF-PI(4,5)P_2. On the other hand, an additional source of fluorescence depolarization for this molecule is the presence of homo-FRET as its fluorescence emission show great overlap with its fluorescence excitation spectra, a pre-requisite for FRET to occur. The Förster radius (R_0) for TF-PI(4,5)P_2,describing the distance at which one acceptor molecule would lead to a 50% chance of FRET, is ~56 Å[72]. While this is a very high value, at the low TF-PI(4,5)P_2 concentrations used here (0.1% of total lipid), only residual FRET takes place between monomers in the absence of clustering. However, when calcium is added to the samples, a dramatic decrease in fluorescence anisotropy is observed, associated with increased FRET within calcium-dependent clusters [50,72].

As expected, at lower temperatures, the fluorescence anisotropy of $PI(4,5)P_2$ with EDTA (monomeric) is higher compared to the anisotropy values in the presence of calcium (Figure 9). This is due to the presence of homoFRET within $Ca^{2+}/PI(4,5)P_2$ clusters, which are absent when EDTA is present[72].

The increase in dynamics observed for monomeric PIP_2 at high temperatures, compensates for the absence of FRET, and at higher temperatures (above 45ºC), the fluorescence anisotropy of the monomeric TF-$PI(4,5)P_2$ is actually lower than that of clustered TF-$PI(4,5)P_2$. In fact, the Δ<r> between 10-70 °C for monomeric TF-$PI(4,5)P_2$ is more than 2-fold the Δ<r> observed for 10-100 µM Ca^{2+} (Figure 9), where nearly all of $PI(4,5)P_2$ is thought to be clustered, as seen above.

These results confirm the recent observation that the order of lipids within the clusters is significantly higher than the order of monomers[59] and is less susceptible to temperature changes. An interesting result is the significant increase in fluorescence anisotropy when samples are brought to 20 °C from 10 °C. These results seem to suggest that at temperatures lower than 20 °C, more efficient clustering takes place, and the reduced depolarization as a result of lower thermal associated dynamics is compensated by an elevated FRET efficiency within $PI(4,5)P_2$ clusters. Nevertheless, further research is necessary to confirm this observation.

Considering the results observed for self-quenching, suggesting that temperature does not significantly affect the extent of PIP_2 aggregation between 20-70 °C, it is expected that FRET should not vary significantly with temperature as well. The observation that the variation of anisotropy with temperature is greater for monomeric PIP_2 than for aggregated PIP_2, suggests that the aggregated PIP_2 is less susceptible to the dynamic variations promoted by the increase in temperature. This result confirms that the PIP_2 aggregates are more ordered than the "bulk" membrane as recently observed[59].

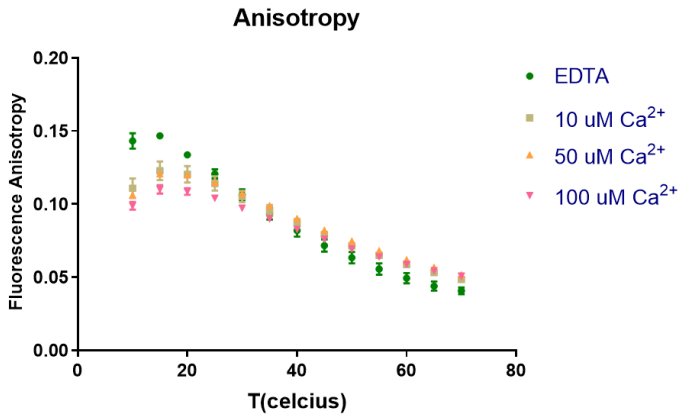

Figure 9. Impact of temperature on the fluorescence anisotropy of TF-$PI(4,5)P_2$. Excitation wavelength was 460 nm and the emission wavelength was set to 510 nm. LUVs containing a mixture of POPC:$PI(4,5)P_2$:TF-$PI(4,5)P_2$ at a 97.4:2.5:0.1 molar ratio in the presence of different calcium concentrations (10, 50 and 100 µM Ca^{2+}). All measurements were taken at range temperatures of 10 - 70 ºC.

3 Effect of cholesterol in the formation of gel phase

3.1 t-pna lifetime

The formation of lipid gel domains in the PM is typically undesirable and their formation is expected to be a rare phenomenon, associated with very specific signalling events or cell death. On the other hand, the formation of lipid gel phases is immediately detected when mixtures of saturated and unsaturated lipids are reconstituted within liposomes with levels of saturated lipids comparable to the normally present in the PM cells eukaryotic cells. In fact, the conspicuous absence of lipid gel domains from the PM in healthy cells is explained by the presence of sterols, which are strong inhibitors of the formation of solid phases.

Recent results from the host laboratory identified that PI(4,5)P_2 with saturated acyl chains, in the presence of calcium, generated calcium-induced clusters in the gel phase. Since the mechanism for gel formation here (triggered by headgroup interactions) is distinct from the conventional mechanism for gel formation (triggered by acyl-chain packing), it remains unclear if cholesterol could play the same role of inhibitor for the formation of PI(4,5)P_2 gel phases in the presence of divalent cations.

In order to clarify this issue, we performed experiments with the membrane probe trans-parinaric acid (tpnA) and with $(16:0)_2$ PI(4,5)P_2. The relative molar fraction of PIP_2 was kept constant (5% of total lipid), while the fraction of cholesterol was varied between 0% and 20%.

The fluorescence lifetime of tpnA is extremely sensitive to the presence of a lipid gel phase, as the membrane probe exhibits an unusual strong preference for incorporation in these solid phases. Additionally, when incorporated in the gel phase, tpnA fluorescence lifetime increases dramatically, and this has been extensively employed as a marker for the formation of lipid gel phases[59,73,74]. A fluorescence decay of tpnA in the presence of calcium is shown in figure 10. In all samples measured, adequate fits were always obtained.

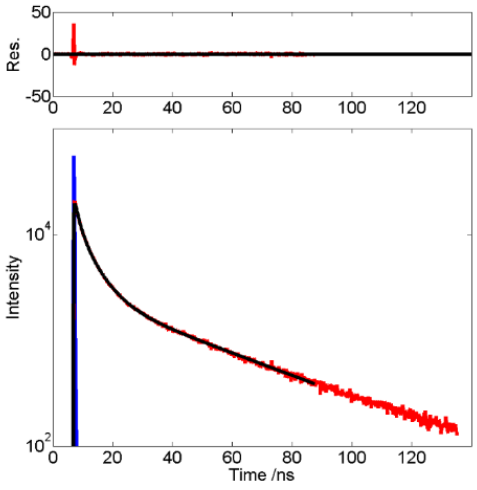

Figure 10. Fluorescence decay of tpnA within liposomes composed of POPC:PI(4,5)P_2 (95:5 % molar ratio) in the presence of 100 µM of Ca^{2+}. Data points are shown in red, while the fitted decay model of a sum of exponentials is shown in black. The instrument response function is shown in blue.

In the absence of calcium, a short (< 4 ns) average fluorescence lifetime is observed for the different percentages of cholesterol (Figure 11), while in the presence of calcium, a marked increase in average fluorescence lifetime takes place, with recovered values above 25 ns.

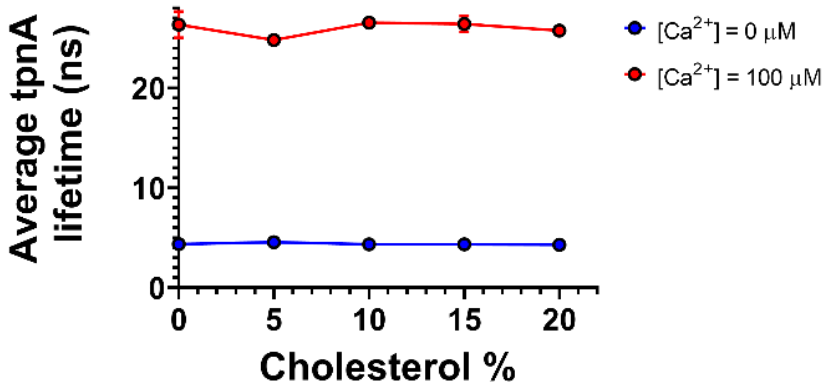

Figure 11. Fluorescence intensity weighed lifetime recovered for tpnA in mixtures of POPC:Chol:PI(4,5)P_2. PI(4,5)P_2 concentration was kept constant at 5%, while the composition of the other two components was varied.

Additionally, the longest lifetime component recovered is shorter than 6ns (Figure 12), well below the threshold of 30 ns that was previously identified as the shorter lifetime of tpnA within gel phases of a ternary diagram[73], confirming that no gel phase is present in the absence of calcium. When calcium was included at 100 μM, the results became dramatically different. In fact, the longest lifetime measured increased to values between 42 and 43 ns, well within the range of fluorescence lifetimes accepted as markers for the formation of the lipid gel phase (Figure 12).

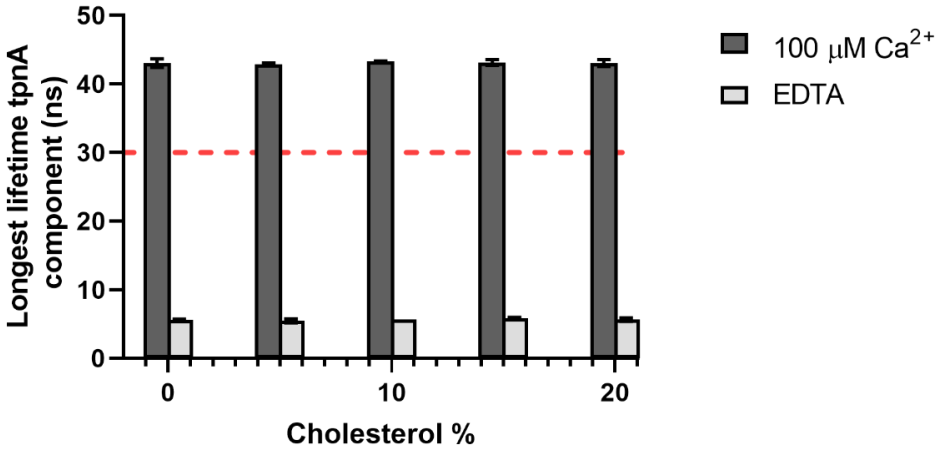

Figure 12. Longest fluorescence lifetime component recovered from the fitting of fluorescence decays of tpnA. Values obtained in the presence of 100 μM Ca^{2+} are shown in dark grey, while values obtained in the absence of calcium (EDTA chelation) are shown in light grey.

While the formation of a lipid phase at all concentrations of cholesterol is evident from figure 11, it is desirable to estimate the approximate fraction of gel phase for each cholesterol concentration, so that the impact of cholesterol can be calculated. Through the measurement of the fraction of the total tpnA fluorescence corresponding to a long fluorescence lifetime (above 30 ns), this quantification is possible (Figure 13). Note that the values shown here do not correspond to the fraction of gel phase, since the quantum yield of tpnA within gel phases is significantly higher than in non-solid phases. Additionally, tpnA does shown preference for incorporation within gel phases. In these conditions, even if the fraction of gel phase present is small, the tpnA fluorescence from these lipid phases will still constitute a very significant fraction of the total tpnA fluorescence. However, any change in gel phase is expected to lead to proportional changes in the contribution of the very long lifetime component and can thus be used to register changes in the fraction of gel phase within the membrane.

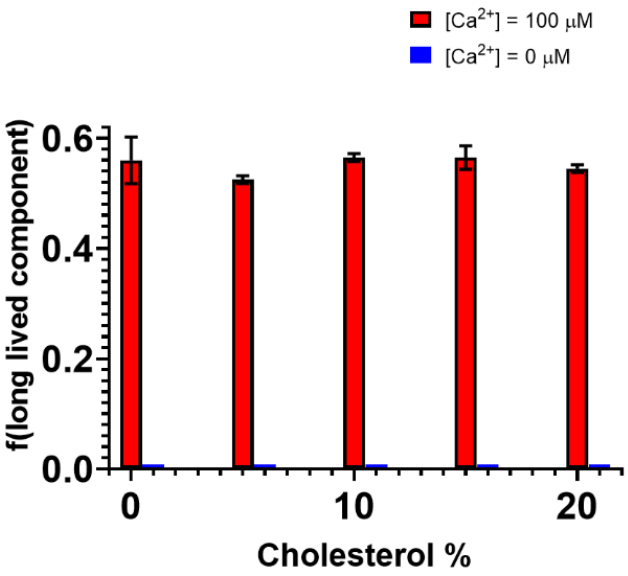

Figure 13. Fraction of the total tpnA fluorescence corresponding to a long fluorescence lifetime (above 30 ns).

From figure 13, it is clear that cholesterol, in the range analysed here, has no impact on the extent of lipid gel phase formed. This is considerably different from the impact of cholesterol on conventional lipid gel phases, which are triggered solely by acyl-chain packing. For $PI(4,5)P_2$, this means that if a sufficient concentration of saturated molecules are present at the PM, the formation of lipid gel nanodomains are likely to be inevitable, as intracellular divalent cation concentration is expected to be sufficient to drive clustering of all free $PI(4,5)P_2$.

3.2 Impact of PI(4,5)P_2 gel phase formation on membrane permeabilization

As seen in previous results, cholesterol does not appear to influence PI(4,5)P_2 gel phase formation and the formation of PI(4,5)P_2 gel nanodomains in the inner leaflet of the PM of living cells is likely inevitable. The impact of the formation of such domains on cellular health remains to be determined. One possible outcome resulting from the presence of these nanodomains would be an increase in membrane permeabilization, with negative results for cellular integrity. In order to evaluate if that is the case, we carried out permeabilization studies with GUVs containing 5% PI(4,5)P_2 and 95% of POPC. We investigated three different PI(4,5)P_2 acyl-chain configurations, so that the impact of gel-like nanodomains could be compared with the impact of unsaturated, fluid nanodomains.

Permeabilization is assessed by the preparation of GUVs and addition of a fluorescent marker such as carboxyfluorescein (CF) to the medium. Initially, the intravesicular medium inside each individual GUV presents no fluorescein. Due to moderate permeability of the vesicle, the fluorophore leaks to the inside compartment over time. The rate at which this occurs can be measured through confocal microscopy of individual GUVs and is proportional to the membrane permeability.

Initial measurements were carried out with GUVs prepared with gel-assisted formation as described in the methods section. However, reproducibility of permeabilization studies in these vesicles was very low. It is possible that some polymer remains associated with GUVs after formation and this could lead to very large variability in permeabilization rates observed for each individual vesicle. Final results presented here were obtained through electroformation as described in the methods section.

Permeabilization was quantified using the following equation:

$$\boldsymbol{Permeabilization}\ (\%) = \frac{\boldsymbol{Int(CF)_{in}}}{\boldsymbol{Int(CF)_{out}}} \tag{6}$$

where $Int(CF)_{in}$describes the average fluorescence intensity inside each vesicle and $Int(CF)_{out}$represents the average fluorescence intensity outside the GUV. Time traces for permeabilization are shown in Figure 15.

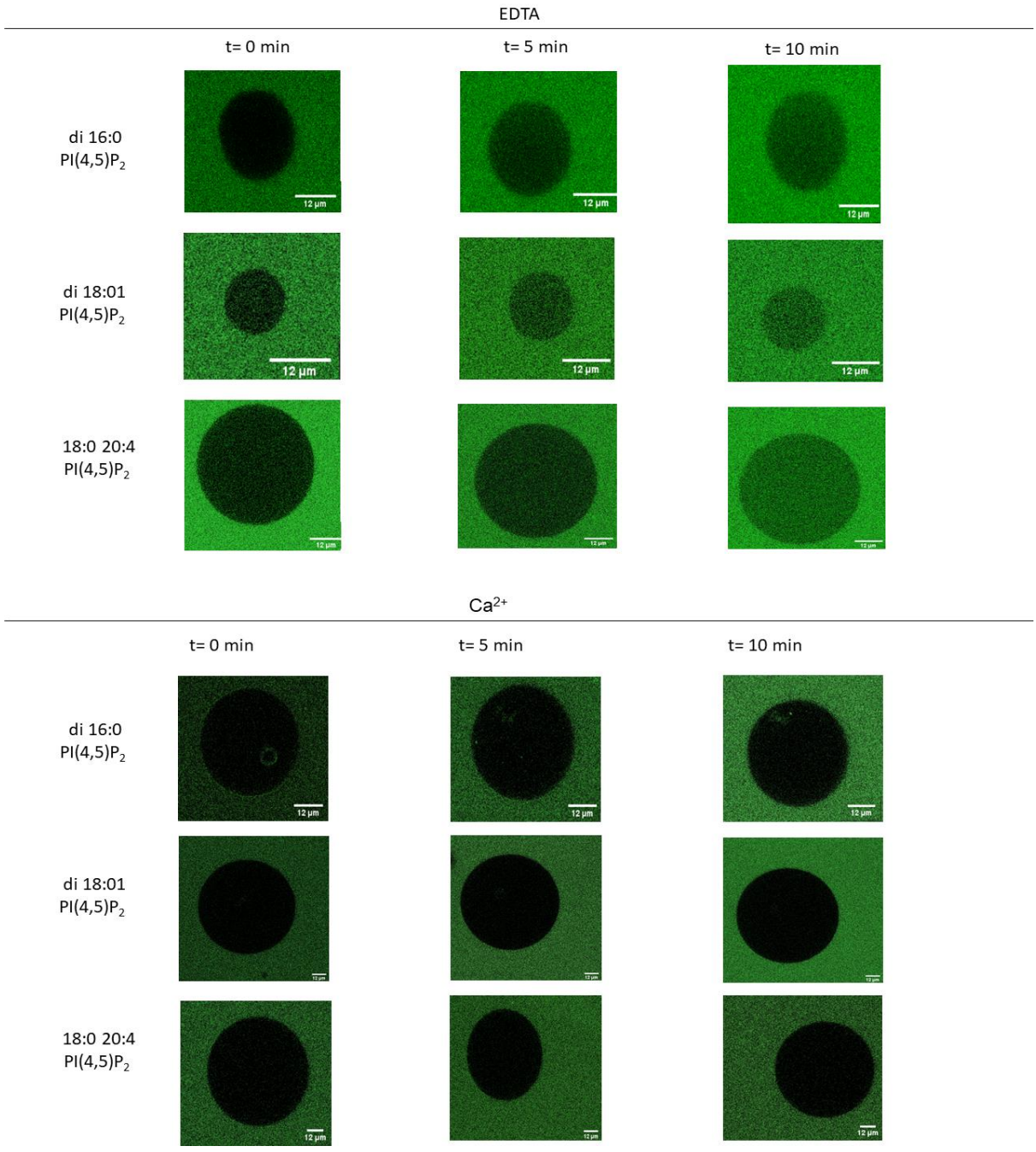

Figure 14. Illustration of the behavior of the carboxyfluorescein in POPC:PI(4,5)P_2 95:5 (mol:mol) GUVs. The experiments were done for the three PI(4,5)P_2 acyl-chain compositions in study in the presence (100 µM Ca^{2+}) and absence (5 mM EDTA) of calcium. Membrane permeabilization is assessed by internalization of carboxyfluorescein within GUVs. Scale bar = 12 µm.

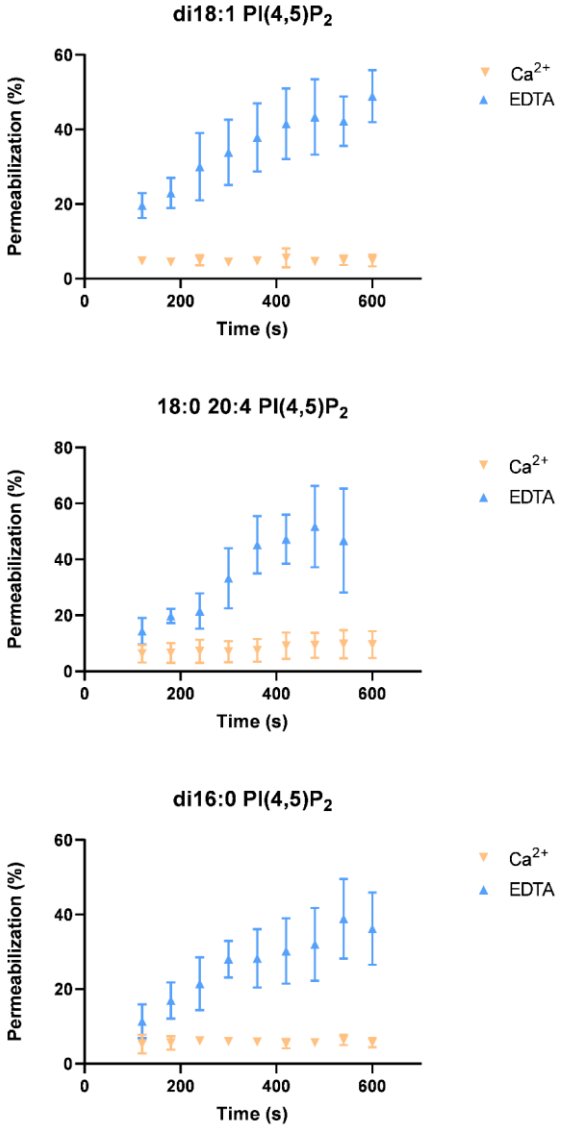

Figure 15. Membrane permeabilization time traces for POPC:PI(4,5)P_2 95:5 (mol:mol) GUVs. The experiments were done for the three PI(4,5)P_2 acyl-chain compositions in study. The percentage of permeabilization values was measured in the presence (100 μM Ca^{2+}, orange) and absence (5 mM EDTA, blue) of calcium. Results are the average of individual GUV permeabilization (N=6) and error bars correspond to standard deviations.

Permeabilization levels obtained for different PI(4,5)P_2 species are very similar, and vesicles without EDTA exhibited almost no permeabilization during the course of the experiment. Surprisingly, in the presence of EDTA, extensive permeabilization took place, also independently of lipid composition. These results seem to suggest that EDTA interacts with lipid membranes increasing permeability, which was not expected. In any case, the results are clear in indicating that the PI(4,5)P_2 nanodomains do not promote significant permeabilization of the lipid membrane. This is also true for the gel domain-inducer 16:0 PI(4,5)P_2.

4 Membrane Tension

4.1 Manipulation of membrane tension

In order to carry out future experiments on the influence of membrane tension on $PI(4,5)P_2$ organization within lipid membranes, conditions for reproducible manipulation of membrane tension of liposomes must first be established. These can be obtained through incubation with fatty acid derivatives or through osmotic stress. In this work we characterized the impact of osmotic stress on membrane tension using a fluorescent sensor for membrane tension called Flipper-TR.

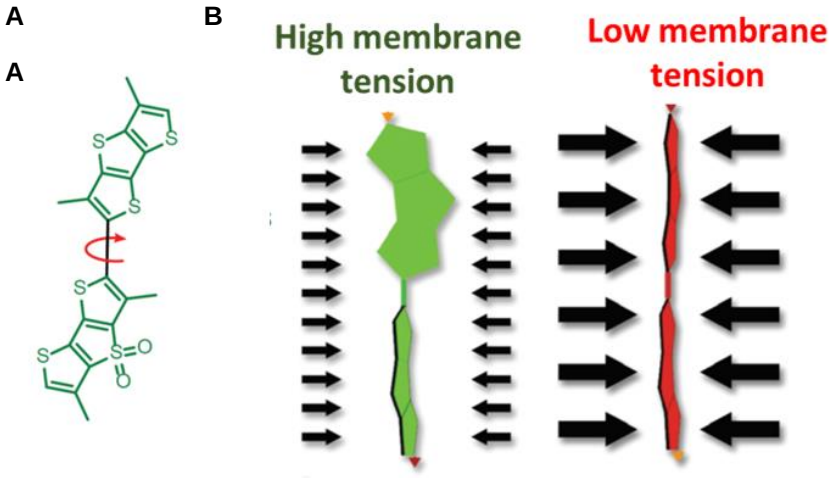

Figure 16. Flipper-TR probe. Chemical structure of FliptR probe; B- Pressure along the axis of the FliptR probe can lead to different changes in fluorescence lifetime upon variation of membrane tension. Adapted from[75]

Flipper-TR presents two twisted dithienothiophene groups[75] (Figure 16.A). Under higher membrane tension and concomitant lower packing pressure, the two groups are twisted out of conjugation by repulsion between the methyls and the endocyclic sulfurs next to the connecting, rotatable bond[75]. As a result, in the absence of complex phase separation, the fluorescence lifetime of FliptR increases for lower membrane tension.

To test the changes in the membrane tension, osmotic shocks were applied to GUVs. GUVs were prepared with a composition of 100% of POPC and 0.5 µM Flipper-TR probe. Flipper-TR was added to preformed vesicles in DMSO. The final percentage of DMSO in solution was kept at 0.5% vol/vol to minimize the impact on membrane structure.

Sucrose concentration inside vesicles was always kept at 200 mM. Different concentrations of glucose in the outer vesicle environment were used to achieve different osmolarity differences between the internal vesicle environment and the outer environment. A hyper-osmotic shock (Δosmolarity = 50 mOsm/L) was obtained using $[Glucose]_{outside}$ = 250 mM and hypo-osmotic shocks (Δosmolarity = - 100

mOsm/L) were obtained using $[Glucose]_{outside}$ = 100 mM. Iso-osmotic conditions (∆osmolarity = 0 mOsm/L) were obtained when $[Glucose]_{outside}$ = 200 mM. Osmolarity of each solution was always confirmed in an osmometer before the experiment.

Since Flipper-TR excited state lifetime is a good sensor for membrane tension, fluorescence lifetime imaging microscopy (FLIM) was employed to obtain individual measurements of Flipper-TR lifetime for each GUV. The fluorescence emission decay curves were obtained by binning all pixel data from each GUV, excluding non-membrane pixels. Decays were fitted with double exponentials, resulting in two lifetimes (τ_1 and τ_2)[75]. The second fluorescence lifetime component of Flipper-TR is responsible for most of the fluorescence and is the most sensitive to changes in membrane tension[75]. In fact, τ_2 is associated with intramolecular charge transfer and thus reports directly on the mechanism by which Flipper-TR senses applied forces[75]. The results shown below correspond to this component.

As expected, upon a hyper-osmotic shock (∆Osmolarity > 0), an increase in Flipper-TR fluorescence lifetime takes place (Figure 17.B). This is due to the decreased area per lipid produced by moderate contraction of the membrane, which increases packing pressure and favours alignment of the two dithienothiophene flippers of Flipper-TR. On the other hand, upon a hypo-osmotic shock (∆Osmolarity < 0), a decrease in Flipper-TR fluorescence lifetime takes place, as the increase in membrane surface area leads to increased membrane tension with concomitant decreased lipid packing and lower alignment of Flipper-TR.

We can them be confident that the osmotic shock conditions chosen for generation of different membrane tensions are effective, and experiments on the behaviour of $PI(4,5)P_2$ in each scenario can be carried out with confidence in the future.

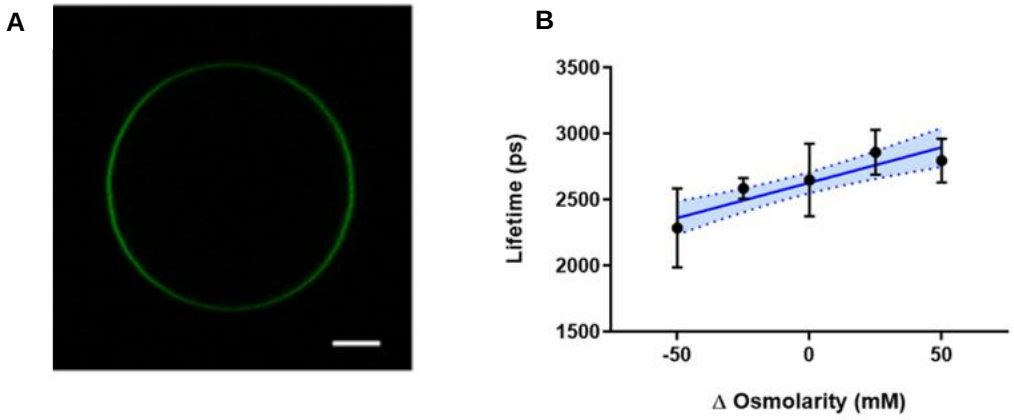

Figure 17. Variation of membrane tension. Images taken from the equatorial plane of POPC:$PI(4,5)P_2$ (95:5 molar ratio) vesicles loaded with Flipper-TR; B- Flipper-TR lifetime vs ∆Osmolarity. ∆Osmolarity = $Osmolarity_{out}$ - $Osmolarity_{in}$. Results are the average of individual GUV permeabilization (N=7) and error bars correspond to standard deviations.

4.2 $PI(4,5)P_2$ incorporation and clustering in GUVs prepared from gel-assisted formation and from electroformation in Pt

GUVs can be obtained by gel-assisted formation or by electroformation in Pt. The latter is known to allow for lower incorporation of heavily charged lipids such as $PI(4,5)P_2$, while the former can result in moderate contamination of vesicles with polymer. In order to ascertain if the method chosen had any impact on $PI(4,5)P_2$ clustering, both methods were used in this section, so that results could be compared. GUVs were composed of 95%POPC:0.5%$PI(4,5)P_2$: 0.5%TF-$PI(4,5)P_2$. The first approach was to measure the TF-$PI(4,5)P_2$ fluorescence lifetime and the membrane intensity for vesicles with and without calcium.

There is a clear difference in TF-$PI(4,5)P_2$ intensity on the membrane of the GUVs prepared from electro- and gel-assisted formation. The gel-assisted method is the one that presents a greater intensity in the membrane (Figure 18.A). A likely justification for the observation is the higher efficiency of incorporation of $PI(4,5)P_2$ when gel-assisted formation is employed.

The fluorescence lifetime of TF-$PI(4,5)P_2$ measured by FLIM is also moderately longer for the gel-assisted method of preparation for the GUVs (Figure 18.B), but the reasons in this case are less clear. Both methods detected significant self-quenching of TF-$PI(4,5)P_2$ within calcium-induced nanodomains when calcium was added, as evident from the decrease in fluorescence lifetimes. Since gel-assisted formation allow for more efficient incorporation of $PI(4,5)P_2$ into GUVs, all further experiments were carried out on GUVs prepared through this method.

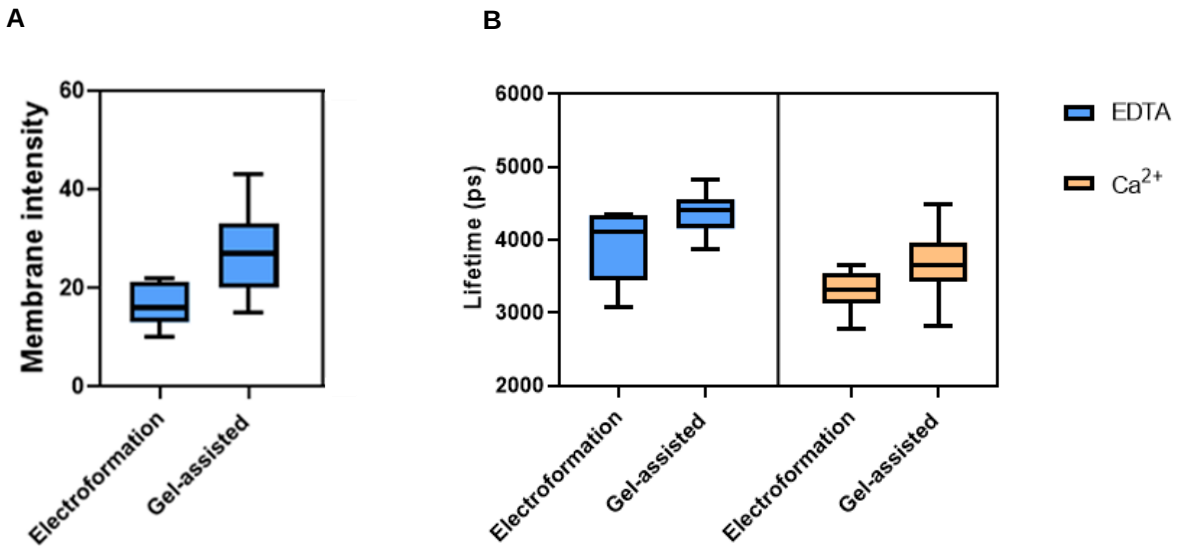

Figure 18. TF-$PI(4,5)P_2$ fluorescence intensity (A) and average lifetimes (B) on GUVs. GUVs were composed of 95%POPC:0.5%$PI(4,5)P_2$: 0.5%TF-$PI(4,5)P_2$. Measurements were carried out through confocal fluorescence microscopy and FLIM, in the presence (orange) and absence of (blue) of free Ca^{2+}.

4.3 Impact of membrane tension on PI(4,5)P_2 clustering

Once more, in order to evaluate PI(4,5)P_2 clustering, TF-PI(4,5)P_2 was employed. As the fluorescence lifetime of this fluorescent analogue is also sensitive to the incorporation within nanodomains, clustering of PI(4,5)P_2 can be followed through FLIM of individual GUVs. FLIM measurements were carried in POPC GUVs loaded with 0.1% or 0.5% of TF-PI(4,5)P_2, in the presence and absence of calcium.

Membrane tension changes were induced as shown before by adding solutions of different osmolarity to the GUVs prepared with 200mM sucrose. Surprisingly, TF-PI(4,5)P_2 fluorescence lifetime increases with osmolarity of the added medium. This is evident in the presence and absence of calcium, suggesting that the changes in fluorescence lifetime are not the result of clustering, as they are also observed for monomeric TF-PI(4,5)P_2. In this context, the observed changes are likely associated to changes in photophysical properties of the Topfluor fluorophore at different membrane tensions. However, further research is necessary to exclude possible artefacts.

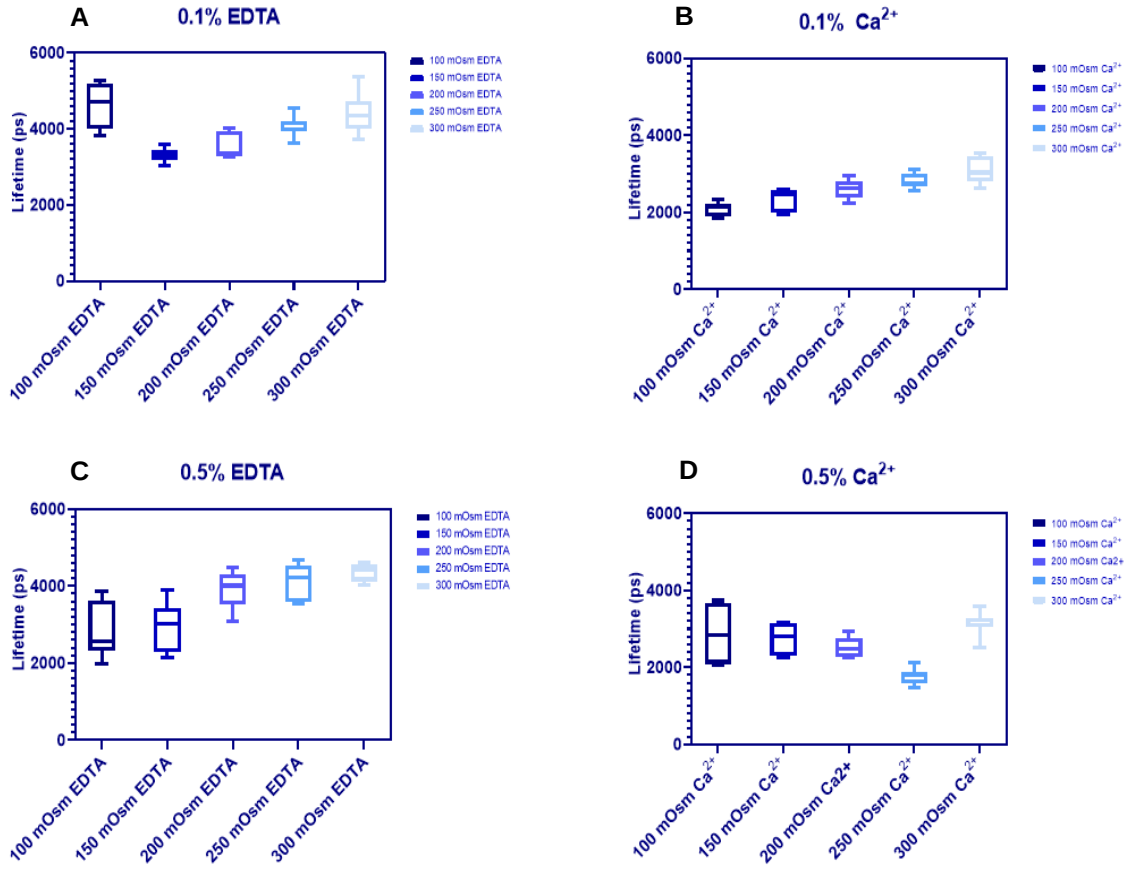

Figure 19. TF-PI(4,5)P_2 average fluorescence lifetimes in POPC GUVs. TF-PI(4,5)P_2 is present at 0.1 %(A and B) or 0.5 (C and D) % molar ratio, and FLIM measurements were carried out in the absence (A and C) and presence (B and D) of calcium. GUVs were prepared at 200 mOsm and the external solution osmolarity was changed from 100-300 mOsm.

A more intriguing result is observed when an external osmolarity of 100 mOsm is employed for GUVs loaded with 0.1% TF-PI(4,5)P_2. In this case, the fluorescence lifetime in the absence of calcium is surprisingly high. This result was highly reproducible indicating that the increased lifetime is not necessarily the result of an artefact. It was also only visible for monomeric PI(4,5)P_2 at 0.1%, as in the presence of calcium, the trend for a decrease in fluorescence lifetime as the membrane tension increases (lower osmolarity of the outer medium) is maintained. Once more, additional studies are necessary to clarify the molecular mechanisms responsible for this change.

When the difference in fluorescence lifetime in the presence and absence of calcium is calculated, results suggest that membrane tension plays no role in regulating PI(4,5)P_2 clustering, as this difference quantified in Figure 20, is somewhat constant, independently of the outer osmolarity, and hence independently of the membrane tension. The exception is the case described above for 100 mOsm, when a significant difference is observed. However, this is more associated with the surprisingly large value of fluorescence lifetime recovered for monomeric TF-PI(4,5)P_2, and thus possibly is not reflective of a modified pattern for PI(4,5)P_2 clustering.

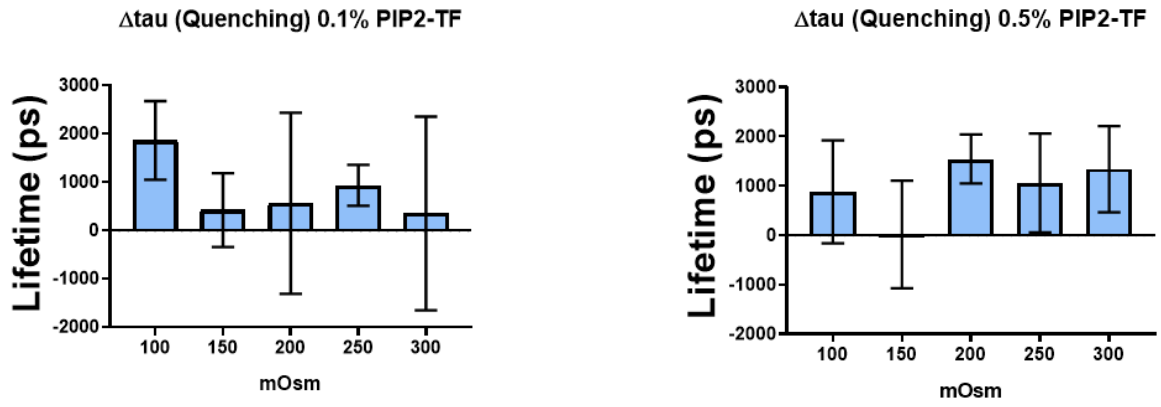

Figure 20. Difference in TF-PI(4,5)P_2 fluorescence lifetime in the presence and absence of calcium, for different osmolarity of the outer medium, reflecting different levels of membrane tension.

One possible justification for the outlier obtained with an outer medium osmolarity of 100 mOsm was that more significant permeabilization of the GUV membrane took place in these conditions. Since EDTA is shown to promote an increase in membrane permeabilization, the membranes exposed to EDTA are likely to undergo a faster equilibration of osmolarity than membranes without the chelating agent. In case the increase in permeability was even higher when a lower osmolarity of the outer medium was employed, the fluorescence lifetime values measured for 100 mOsm in the outer medium (corresponding to high membrane tension), could be reflecting a fully permeabilized membrane, unlike what is observed for other osmolarities. To test if this was the case, the same permeabilization measurements carried out before were tested for this condition and compared with the results obtained for osmotic equilibrium (200 mOsm in the outer medium) (Figure 21). Results clearly demonstrate that the excessive permeabilization observed in the presence of EDTA for both conditions is comparable. In

this way, the TF-PI(4,5)P_2 outlier value obtained for 100 mOsm outer osmolarity is not the result of more efficient membrane permeabilization.

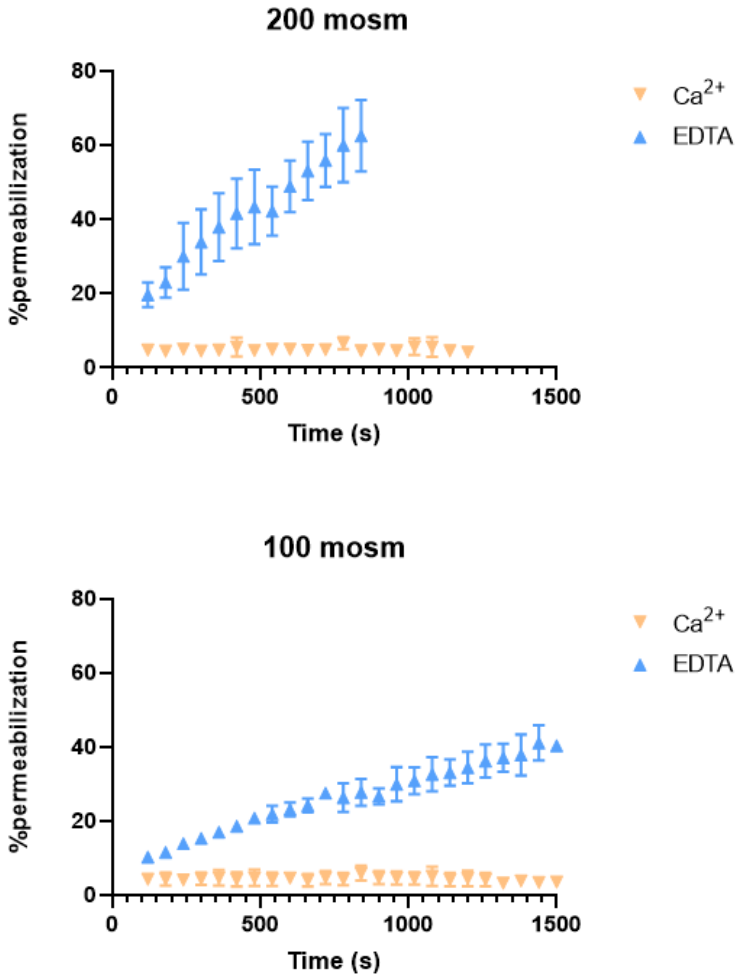

Figure 21. The carboxyfluorescein (CF) permeabilization study was carried out in GUVs composed of POPC:PI(4,5)P_2 95:5 mol:mol. The percentage of permeabilization values were measured in the presence (100 µM Ca^{2+}, orange) and absence (5 mM EDTA, blue) of calcium.

IV. Discussion

It is remarkable that a single lipid class such as PI(4,5)P_2, which is present at low and nearly constant steady-state levels, can act as an important regulator in so many different, yet simultaneous, signalling pathways[59,76]. The current understanding is that lateral organization of PI(4,5)P_2 within the PM is critical to that end. In this regard, PI(4,5)P_2 exhibits a complex lateral organization at the PM, with considerable variability between cells types[77]. The presence of nanodomains enriched in the lipid, will have considerable consequences for PM organization, as the protein profile and activity within these domains will be radically different from the bulk PM.

Recently, this lipid was shown by FRET microscopy to be enriched in nanoscale compartments in HeLa cells, while in HEK293T cells, no evidence for compartmentalization was identified[77]. Importantly, the compartmentalization observed in HeLa cells was almost entirely dependent on the presence of an intact cytoskeleton[77] (Figure 22). It is possible that the recruitment of kinases to membrane domains of restricted diffusion due to the presence of actin-based fences, could be sufficient to maintain these nanodomains, but in any case, the maintenance of these structures is bound to have large energetic costs for the cell.

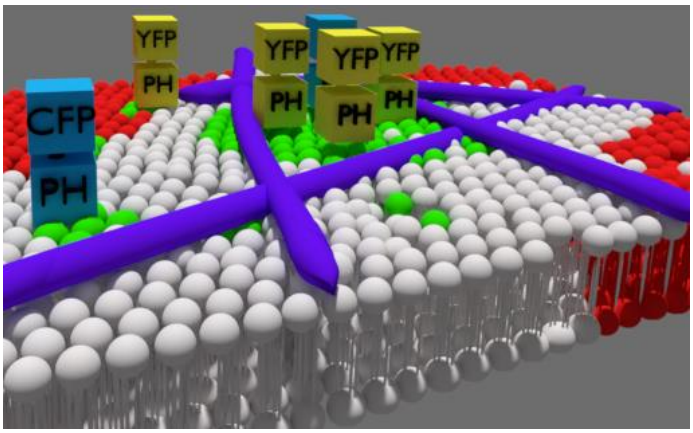

Figure 22. Illustration of distribution of PI(4,5)P_2 (green phospholipids) and PI(4,5)P2 binding pleckstrin homology domains (PH) fused with fluorescent proteins (PH-FP) [82].The cytoskeleton (purple structures) was found to be the critical factor determining formation of PI(4,5)P_2 enriched nanodomains.

A strong tendency of PI(4,5)P_2 to stablish nanoclusters in the presence of divalent cation (Ca^{2+},Mg^{2+}) concentrations within physiological levels has been recently confirmed[59,72,78,79]. In this way, it seems that PI(4,5)P_2 is not entirely free for interaction when unbound from protein partners, but exists in a monomer-divalent cation induced cluster equilibria. Results obtained with liposomes in the presence of magnesium, suggest that most of PI(4,5)P_2 is likely to be incorporated within clusters when exposed to typical free intracellular magnesium concentrations. This is to have obvious consequences for PI(4,5)P_2-protein interactions within the PM. Proteins exhibiting low binding affinity for PI(4,5)P_2 could be strongly attracted to PI(4,5)P_2 nanoclusters, while the high concentration of divalent cations in these structures will inevitably lead to some charge shielding with impact in protein affinity. In this scenario, the triggering of PI(4,5)P2 clustering could offer an additional level of regulation for PI(4,5)P2 signalling[59].

Importantly, generation of $PI(4,5)P_2$ rich nanodomains such as the ones observed in the PM of living cells, could become energetically more favourable when $PI(4,5)P_2$ is mostly found clustered, as diffusion from the clustering site is minimized and restriction of $PI(4,5)P_2$ cluster diffusion by cytoskeleton barriers is likely to be more effective than restriction of diffusion for monomeric $PI(4,5)P_2$. In this case, generating $PI(4,5)P_2$ enriched nanodomains is likely to be more economic energetically.

$PI(4,5)P_2$ clustering has been shown to be more effective when the bulk membrane exhibited higher order[78]. However, beyond this factor, almost no information is available regarding the modulators of $PI(4,5)P_2$ clustering. Two likely physical modulators for $PI(4,5)P_2$ clustering were temperature and membrane tension.

Regarding the impact of temperature, both $PI(4,5)P_2$-divalent cation and multivalent $PI(4,5)P_2$-Ca^{2+}-$PI(4,5)P_2$ interactions were expected to be hampered by an increase in thermal-associated dynamics. Additionally, $PI(4,5)P_2$ membrane surface area was shown to be much more impacted by temperature than other lipid classes, and this was rationalized to be associated with a disruption of the hydrogen boding network as temperature increases [80]. Since the hydrogen bonding network is critical for nanocluster formation, temperature could thus act as a strong modulator of $PI(4,5)P_2$ clustering. The result shown here indicate that in the range of 20-70 °C, temperature has almost no impact on the stability of calcium-induced $PI(4,5)P_2$ clusters. This is surprising, since other types of lipid phase separation observed in bio membranes are typically temperature dependent. This is the case for liquid-ordered/liquid disordered, or fluid/gel phase separation.

Intriguingly, significant changes in behaviour of the fluorescent analogue of $PI(4,5)P_2$ were evident when samples were cooled to 10 °C. Fluorescence intensity and anisotropy values decreased moderately at this temperature suggesting more efficient clustering and FRET within these clusters. This is likely reflecting the proximity to the transition temperature of POPC (T_m = -2 °C), as $PI(4,5)P_2$ has been shown to cluster more effectively when embedded in more ordered membranes. In this way, with the exception of temperatures close to the transition temperature of the bulk lipid, $PI(4,5)P_2$ clusters were stable throughout the temperature range analysed.

The impact of membrane tension on $PI(4,5)P_2$ clustering is more unpredictable. A recent study has identified $PI(4,5)P_2$ as the sensor for membrane tension changes in the PM[55]. Changes in membrane tension, lead to an enrichment of $PI(4,5)P_2$ in to specific domains, which then triggered a signalling response. However, the mechanism through which this occurred is still obscure. Since changes in phospholipid surface area are observed when $PI(4,5)P_2$ interacts with either calcium or magnesium[80,81], it is conceivable that clustering of $PI(4,5)P_2$ could be impacted upon changes in lateral membrane pression. The results shown here seem to negate such an idea. In fact, the fluorescence lifetime of the $PI(4,5)P_2$ analogue remained roughly insensitive to different osmotic shocks which are expected to give rise to different degrees of membrane tension.

Clustering of 16:0 $PI(4,5)P_2$ has been recently show to induce the formation of a solid gel-like phase, even at extremely low concentrations of $PI(4,5)P_2$ (1%)[59]. Other gel phases, such as the ones originating for saturated sphingomyelins, are generally undesirable at the PM and their formation is

highly limited by the presence of sterols. Sine the mechanism through which both solid phases are formed is different (acyl-chain packing for conventional gel pashes and headgroup promoted interactions for saturated PI(4,5)P_2), it remained unclear whether cholesterol could also inhibit the formation of the recently described 16:0 PI(4,5)P_2 gel phases. Our results shown here also ruled out a role of cholesterol in mitigating the formation of these solid gel-like membrane domains. Since cholesterol was show not be effective in disrupting the formation of these phases, the presence of saturated PI(4,5)P_2 would invariably lead to the formation of undesirable gel phases at the PM. It is interesting then that this lipid is relatively rare. In fact, the dominant polyunsaturated PI(4,5)P_2 specie in animal cells, with 18:0,20:4 acyl-chains, might have been evolutionary selected to reduce ordering of PI(4,5)P_2 clusters, and in liposomes, the polyunsaturated PI(4,5)P_2 was shown to abrogate the formation of the 16:0 PI(4,5)P_2 gel phase[59], seemingly confirming this hypothesis.

Overall, the formation of PI(4,5)P_2 nanoclusters was shown to be largely insensitive to both physical and chemical factors tested (Figure 23). These results suggest that PI(4,5)P_2 clustering is not prone to regulation. The tight binding between the phospholipid, divalent cations and other PI(4,5)P_2 molecules do not seem to be significantly impaired by any of the factors tested, namely the physical properties temperature and membrane tension. It is possible then that PI(4,5)P_2 clustering is constitutively present and cannot be disrupted. In this model, monomeric PI(4,5)P_2 would be seldomly observed, and this phospholipid would be either bound to a protein partner or part of a nanodomain. If that is the case, the interactions between PI(4,5)P_2 binding proteins and the phospholipid would be exclusively dictated by the affinity of the protein to the clustered form of PI(4,5)P_2. Since nearly all literature on PI(4,5)P_2-protein interactions has exclusively focused on the affinity of the latter for monomeric PI(4,5)P_2, the field could require a revision to reflect this.

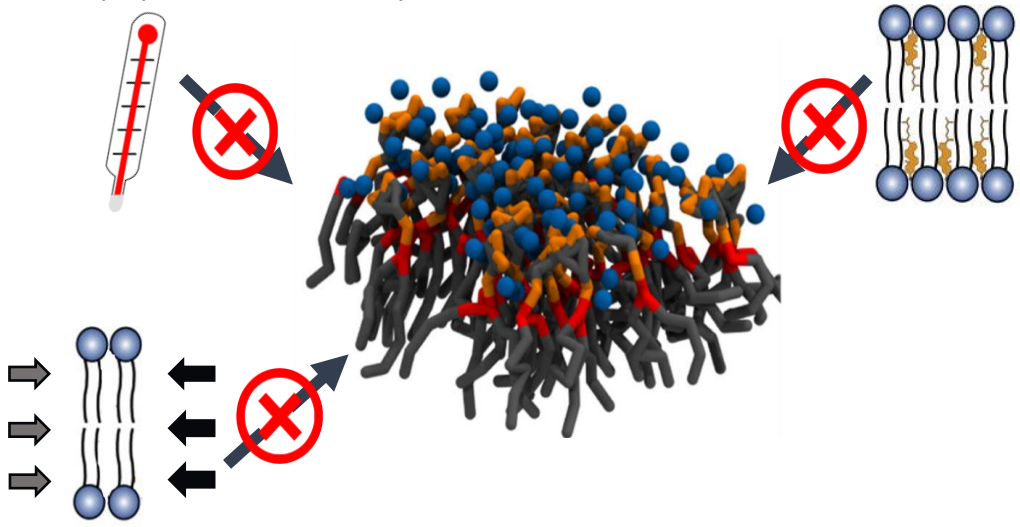

Figure 23 Effect of the chemical and physical factors in the formation on PI(4,5)P_2 clusters. Formation of PI(4,5)P_2 nanoclusters was shown to be largely insensitive to both physical and chemical factors tested.

V. References

1. Nelson,D.L & Cox M. *Lehninger Principles of Biochemistry Sicth Edition*.; 2013.

2. Gorter BYE. On bimolecular layers of lipoids on the chromo- cytes of the blood. *J Exp Med*. 1925;41:439-443.

3. Singer, S. J., & Nicolson GL. The Fluid Mosaic Model of the Structure of Cell Membranes. *Science (80-)*. 1972;175(4023):720-731.

4. Characterization MS, Edidin M. Lipids on the frontier : a century of cell-membrane bilayers. *Nat Rev Mol Cell Biol*. 2003;4(5):414-418.

5. Nicolson GL. The Fluid - Mosaic Model of Membrane Structure: Still relevant to understanding the structure, function and dynamics of biological membranes after more than 40 years. *Biochim Biophys Acta - Biomembr*. 2014;1838(6):1451-1466.

6. Donato P, Dugo P, Mondello L. *Separation of Lipids*. Elsevier Inc.; 2013. doi:10.1016/B978-0-12-415806-1.00009-7

7. Holthuis JCM, Menon AK. Lipid landscapes and pipelines in membrane homeostasis. *Nature*. 2014;510(7503):48-57. doi:10.1038/nature13474

8. Eeman M, Deleu M. From biological membranes to biomimetic model membranes. *BiotechnolArgonSocEnviron*. 2010;14(4):719-736.

9. Bagatolli LA, Ipsen JH, Simonsen AC, Mouritsen OG. An outlook on organization of lipids in membranes: Searching for a realistic connection with the organization of biological membranes. *Prog Lipid Res*. 2010;49(4):378-389.

10. de Almeida RFM, Fedorov A, Prieto M. Sphingomyelin/phosphatidylcholine/cholesterol phase diagram: boundaries and composition of lipid rafts. *Biophys J*. 2003;85(4):2406-2416.

11. Elson EL, Fried E, Dolbow JE, Genin GM. Phase separation in biological membranes: integration of theory and experiment. *Annu Rev Biophys*. 2010;39:207-226.

12. Bacia K, Schuette CG, Kahya N, Jahn R, Schwille P. SNAREs Prefer Liquid-disordered over " Raft " (Liquid-ordered) Domains When Reconstituted into Giant Unilamellar Vesicles. *J Biol Chem*. 2004;279(36):37951-37955.

13. Pike LJL. Rafts defined: a report on the Keystone Symposium on Lipid Rafts and Cell Function. *J Lipid Res*. 2006;47(7):1597-1598.

14. Simons K, Van Meer G. Lipid sorting in epithelial cells. *Biochemistry*. 1988;27(17):6197-6202.

15. Simons K, Ikonen E. Functional rafts in cell membranes. *Nature*. 1997;387(6633):569-572.

16. Baumgart T, Hammond AT, Sengupta P, et al. Large-scale fluid/fluid phase separation of proteins and lipids in giant plasma membrane vesicles. *Proc Natl Acad Sci U S A*. 2007;104(9):3165-3170.

17. Patton RG. Caveolae and caveolins. *Curr Opin Cell Biol*. 1996;8(4):542-548.

18. Florent Bender, Margarita Montoya VM, Lisette Leyton AFGQ. Caveolae and caveolae-like membrane domains in cellular signaling and disease: Identification of downstream targets for the tumor suppressor protein caveolin-1. *Biol Res*. 2002;35(2):139-150.

19. Lomholt MA. Imaging approaches for analysis of cholesterol distribution and dynamics in the plasma membrane. *Chem Phys Lipids*. 2016;199:106-135.

20. Jacobson K, Liu P, Lagerholm BC, Oxford IC, Way H, Kingdom U. The lateral organization and mobility of plasma membrane components. *Cell*. 2019;177(4):806-819. doi:10.1016/j.cell.2019.04.018.The

21. Pomorski T, Holthuis JCM, Herrmann A, Meer G Van. Tracking down lipid flippases and their biological functions. *J Cell Sci*. 2004;117(6):805-813.

22. Devaux PF. Lipid transmembrane asymmetry and flip-flop in biological membranes and in lipid bilayers. *Curr Opin Stuctural Biol*. 1993;3(2):489-494.

23. Chan Y-HM, Boxer SG. Model membrane systems and their applications. *Curr Opin Chem Biol*. 2007;11(6):581-587.

24. Przybylo M, Sy J, Humpolı J, Zan A, Hof M, Heyro J V. Lipid Diffusion in Giant Unilamellar Vesicles Is More than 2 Times Faster than in Supported Phospholipid Bilayers under Identical Conditions. *Langmuir*. 2006;22(22):9096-9099.

25. Patil YP, Jadhav S. Novel methods for liposome preparation. *Chem Phys Lipids*. 2014;177:8-18.

26. Yoo J, Cui Q. Curvature Generation and Pressure Profile Modulation in Membrane by Lysolipids : Insights from Coarse-Grained Simulations. *Biophysj*. 2009;97(8):2267-2276.

27. Bhatia T, Cornelius F, Ipsen JH. Exploring the Raft-hypothesis by probing planar bilayer patches of free-standing giant vesicles at nanoscale resolution, with and without Na,K-ATPase. *BBA - Biomembr*. 2016;1858(12):3041-3049.

28. Bagatolli LA, Needham D. Quantitative optical microscopy and micromanipulation studies on the lipid bilayer membranes of giant unilamellar vesicles. *Chem Phys Lipids*. 2014;181:99-120.

29. Heinemann F, Betaneli V, Thomas FA, Schwille P. Quantifying Lipid Di ff usion by Fluorescence Correlation Spectroscopy: A Critical Treatise. *Langmuir*. 2012;28(37):13395-13404.

30. Viaud J, Mansour R, Antkowiak A, et al. Biochimie Phosphoinositides : Important lipids in the coordination of cell dynamics. *Biochimie*. 2016;125:250-258.

31. Vicinanza M, Angelo GD, Campli A Di, et al. Phosphoinositides as regulators of membrane trafficking in health and disease. *Cell Mol Life Sci*. 2008;65:2833-2841. doi:10.1007/s00018-008-8353-2

32. Mandal K. Review of PIP2 in Cellular Signaling , Functions and Diseases. 2020;10:1-20.

33. Borges-Araujo L; Fernandes F. Structure and Lateral Organization of Phosphatidylinositol 4,5-bisphosphate. *Molecules*. 2020;25(17):1-17.

34. Levin R, Grinstein S, Schlam D. Phosphoinositides in phagocytosis and macropinocytosis. *Mol Cell Biol Lipids*. 2015:805-823.

35. Di Paolo G, De Camilli P. Phosphoinositides in cell regulation and membrane dynamics. *Nature*. 2006;443(7112):651-657.

36. Martin TFJ. PI (4 , 5) P 2 regulation of surface membrane traffic. *Curr Opin Cell Biol*. 2001;13(4):493-499.

37. Toker A. The synthesis and cellular roles of phosphatidylinositol 4,5-bisphosphate. *Curr Opin Cell Biol*. 1998;10(2):254-261.

38. Kwiatkowska K. One lipid , multiple functions : how various pools of PI (4 , 5) P 2 are created in the plasma membrane. *Cell Mol Life Sci*. 2010;67(23):3927-3946.

39. McLaughlin S, Wang J, Gambhir A, Murray D. PIP(2) and proteins: interactions, organization, and information flow. *Annu Rev Biophys Biomol Struct*. 2002;31:151-175.

40. Xu C, Wan Z, Shaheen S, Wang J, Yang Z, Liu W. A PI (4 , 5) P2 - derived " gasoline engine model " for the sustained B cell receptor activation. *Immunol Rev*. 2019;291(1):75-90.

41. Levental I, Christian D a, Wang Y, et al. Calcium-dependent lateral organization in phosphatidylinositol 4,5-bisphosphate (PIP2)- and cholesterol-containing monolayers. *Biochemistry*. 2009;48(34):8241-8248.

42. Diederichsen U, Jahn R. Membrane protein sequestering by ionic protein– lipid interactions. *Nature*. 2011;479(7374):552-555.

43. Wang J, Richards DA. Segregation of PIP2 and PIP3 into distinct nanoscale regions within the plasma membrane. *Biol Open*. 2012;1(9):857-862.

44. Clapham DE. Calcium signaling. *Cell*. 1995;80(2):259-268.

45. Grubbs RD. Intracellular magnesium and magnesium buffering. *BioMetals*. 2002;15(3):251-259.

46. Trapani V, Farruggia G, Marraccini C, Iotti S, Cittadini A, Wolf FI. Intracellular magnesium detection: imaging a brighter future. *Analyst*. 2010;135:1855-1866.

47. Wang Y-H, Collins A, Guo L, et al. Divalent cation-induced cluster formation by polyphosphoinositides in model membranes. *J Am Chem Soc*. 2012;134(7):3387-3395.

48. Ellenbroek WG, Wang Y, Christian DA, Discher DE, Janmey PA, Liu AJ. Divalent Cation-Dependent Formation of Electrostatic PIP 2 Clusters in Lipid Monolayers. *Biophys J*. 2011;101(9):2178-2184.

49. Sarmento MJ, Coutinho A, Fedorov A, Prieto M, Fernandes F. Ca2 + induces PI(4,5)P2 clusters on lipid bilayers at physiological PI(4,5)P2 and Ca2 + concentrations. *Biochim Biophys Acta (BBA)- Biomembr*. 2014;1838(3):822-830.

50. Sarmento MJ, Coutinho A, Fedorov A, Prieto M, Fernandes F. Membrane order is a key regulator of divalent cation-induced clustering of PI(3,5)P2 and PI(4,5)P2. *Langmuir*. 2017;33(43):12463-12477. doi:10.1021/acs.langmuir.7b00666

51. Prieto M, Lu F. Quantification of protein – lipid selectivity using FRET. *Eur Biophys J*. 2009;39(4):565-578.

52. Balla T, Introduction I. Phosphoinositides: Tiny Lipids With Giant Impact on Cell Regulation. *Physiol Rev*. 2013;93(3):1019-1137.

53. Janmey PA, Kinnunen PKJ. Biophysical properties of lipids and dynamic membranes. *Trends Cell Biol*. 2006;16(10):538-546. doi:10.1016/j.tcb.2006.08.009

54. Loh J, Chuang M, Lin S, Joseph J, Su Y, Hsieh T. An acute decrease in plasma membrane tension induces macropinocytosis via PLD2 activation. *J Cell Sci*. 2019;132:1-14.

55. Riggi M, Niewola-Staszkowska K, Chiaruttini N, et al. Decrease in plasma membrane tension triggers PtdIns(4,5)P 2 phase separation to inactivate TORC2. *Nat Cell Biol*. 2018;20(9):1043-1051. doi:10.1038/s41556-018-0150-z

56. Ebner, M., & Haucke V. Mechanical signals regulate TORC2 activity. *Nat Cell Biol*. 2018;20(9):994-995.

57. Prieto JA, Estruch F, Córcoles-sáez I, et al. Pho85 and PI(4,5)P2 regulate different lipid metabolic pathways in response to cold. *BBA - Mol Cell Biol Lipids*. 2019.

58. Levental I, Cebers A, Janmey PA. Combined Electrostatics and Hydrogen Bonding Determine PIP(2) Intermolecular Interactions. *J Am Chem Soc*. 2008;130(28):9025-9030.

59. Borges-Araújo, L., M.M. Domingues, A. Fedorov, N.C. Santos, M.N. Melo, and F. Fernandes. 2021. Acyl-chain saturation regulates the order of phosphatidylinositol 4,5-bisphosphate nanodomains. Commun. Chem. 4:164.60.

61. Castro BM, Silva LC, Fedorov A, de Almeida RFM, Prieto M. Cholesterol-rich fluid membranes solubilize ceramide domains: implications for the structure and dynamics of mammalian intracellular and plasma membranes. *J Biol Chem*. 2009;284(34):22978-22987.

62. Wiederschain GY. The Molecular Probes handbook. A guide to fluorescent probes and labeling technologies. *Biochem*. 2011;76(11):1276-1276.

63. Haugland, R. P., Spence, M. T. Z. & Johnson ID. Handbook of fluorescent probes and research chemicals. 1996.

64. McClare CW. An accurate and convenient organic phosphorus assay. *Anal Biochem*. 1971;39(2):527-530.

65. Haugland RP. *The Handbook: A Guide to Fluorescent Probes and Labeling Technologies*. (Probes M, ed.). n/a; 2005.

66. de Almeida RFM, Loura LMS, Fedorov A, Prieto M, Loura MS, Almeida RFM De. Lipid rafts have different sizes depending on membrane composition: a time-resolved fluorescence resonance energy transfer study. *J Mol Biol*. 2005;346(4):1109-1120.

67. Weinberger A. Gel-Assisted Formation of Giant Unilamellar Vesicles. *Biophysical*. 2013;105(July):154-164.

68. Angelova MI, Dimitrov DS. Liposome Electro formation. *Faraday Discuss Chem SOC*. 1986;81:303-311.

69. Loura LMS, Fedorov A, Prieto M. Partition of membrane probes in a gel/fluid two-component lipid system: a fluorescence resonance energy transfer study. *Biochim Biophys Acta*. 2000;1467(1):101-112.

70. ROBERT J. HUNTER. *Zeta Potential in Colloid Science: Principles and Applications*. Academic Press; 1981.

71. Borges-Araújo L, Fernandes F, Borges-Araujo L; Fernandes F. Structure and Lateral Organization of Phosphatidylinositol 4,5-bisphosphate. *Molecules*. 2020;25(17):3885.

72. Sarmento MJ, Coutinho A, Fedorov A, Prieto M, Fernandes F. Ca2+ induces PI(4,5)P2 clusters on lipid bilayers at physiological PI(4,5)P2 and Ca2+ concentrations. *Biochim Biophys Acta - Biomembr*. 2014;1838(3):822-830.

73. Nyholm TKMM, Lindroos D, Westerlund B, Slotte JP. Construction of a DOPC/PSM/cholesterol phase diagram based on the fluorescence properties of trans -parinaric acid. *Langmuir*. 2011;27(13):8339-8350.

74. Silva L, De Almeida RFM, Fedorov A, Matos APA, Prieto M. Ceramide-platform formation and -induced biophysical changes in a fluid phospholipid membrane. *Mol Membr Biol*. 2006;23(2):137-148.

75. Colom A, Derivery E, Soleimanpour S, et al. A fluorescent membrane tension probe. *Nat Chem*. 2018;10(11):1118-1125.

76. Kwiatkowska K. One lipid, multiple functions: how various pools of PI(4,5)P(2) are created in the plasma membrane. *Cell Mol life Sci*. 2010;67(23):3927-3946.

77. Sarmento MJ, Borges-Araújo L, Pinto SN, et al. Quantitative FRET microscopy reveals a crucial role of cyto-skeleton in promoting PI(4,5)P2 confinement. *Int J Mol Sci*. 2021;(in press).

78. Sarmento MJ, Coutinho A, Fedorov A, Prieto M, Fernandes F. Membrane Order Is a Key

Regulator of Divalent Cation-Induced Clustering of PI(3,5)P 2 and PI(4,5)P 2. *Langmuir*. 2017;33(43):12463-12477.

79. Wen Y, Vogt VM, Feigenson GW. Multivalent Cation-Bridged PI(4,5)P2 Clusters Form at Very Low Concentrations. *Biophys J*. 2018;114(11):2630-2639.

80. Levental I, Janmey PA, Cēbers a, Cebers A. Electrostatic Contribution to the Surface Pressure of Charged Monolayers Containing Polyphosphoinositides. *Biophys\ J*. 2008;95(3):1199-1205.

81. Bilkova E, Pleskot R, Rissanen S, et al. Calcium Directly Regulates Phosphatidylinositol 4,5-Bisphosphate Headgroup Conformation and Recognition. *J Am Chem Soc*. 2017;139(11):4019-4024.

82. Sarmento MJ, Araújo LB, Pinto SN, et al. Quantitative FRET Microscopy Reveals a Crucial Role of Cytoskeleton in Promoting PI(4,5)P2 Confinement. *Int J Mol Sci*. 2021.